HHS Public Access

Author manuscript

Cell Rep. Author manuscript; available in PMC 2024 June 23.

Published in final edited form as:

Cell Rep. 2024 May 28; 43(5): 114140. doi:10.1016/j.celrep.2024.114140.

Sex-specific expression of distinct serotonin receptors mediates stress vulnerability of adult hippocampal neural stem cells in mice

Yan-Jia Luo[1,2,3,6], **Hechen Bao**[1,2,6], **Andrew Crowther**[1,4,6], **Ya-Dong Li**[1,2,5], **Ze-Ka Chen**[1,2], **Dalton S. Tart**[1], **Brent Asrican**[1,2], **Libo Zhang**[1], **Juan Song**[1,2,7,*]

[1]Department of Pharmacology, University of North Carolina, Chapel Hill, NC 27599, USA

[2]Neuroscience Center, University of North Carolina, Chapel Hill, NC 27599, USA

[3]Department of Anesthesiology, Shanghai Ninth People's Hospital, Shanghai Jiao Tong University School of Medicine, Shanghai 200011, China

[4]Neuroscience Curriculum, University of North Carolina, Chapel Hill, NC 27599, USA

[5]Songjiang Research Institute, Songjiang Hospital Affiliated with Shanghai Jiao Tong University School of Medicine, Shanghai Key Laboratory of Emotions and Affective Disorders, Shanghai 201699, China

[6]These authors contributed equally

[7]Lead contact

SUMMARY

Women are more vulnerable to stress and have a higher likelihood of developing mood disorders. The serotonin (5HT) system has been highly implicated in stress response and mood regulation. However, sex-dependent mechanisms underlying serotonergic regulation of stress vulnerability remain poorly understood. Here, we report that adult hippocampal neural stem cells (NSCs) of the Ascl1 lineage (Ascl1-NSCs) in female mice express functional 5HT1A receptors (5HT1ARs), and selective deletion of 5HT1ARs in Ascl1-NSCs decreases the Ascl1-NSC pool only in females. Mechanistically, 5HT1AR deletion in Ascl1-NSCs of females leads to 5HT-induced depolarization mediated by upregulation of 5HT7Rs. Furthermore, repeated restraint stress (RRS) impairs Ascl1-NSC maintenance through a 5HT1AR-mediated mechanism. By contrast, Ascl1-NSCs in males express 5HT7R receptors (5HT7Rs) that are downregulated by RRS, thus maintaining the

*Correspondence: juansong@email.unc.edu.

AUTHOR CONTRIBUTIONS

J.S. led the project and wrote the manuscript. Y.-J.L., H.B., and A.C. designed and performed the experiments and contributed to manuscript writing. Y.-J.L. performed slice electrophysiology, analyzed *in vivo* functional data, and performed *in situ* hybridization. H.B. and D.S.T. analyzed *in vivo* functional analysis. A.C. acquired confocal images, analyzed *in vivo* functional data, and performed *in situ* hybridization. B.A. assisted with slice electrophysiological recording. Y.-D.L. assisted with taking confocal images and animal breeding. Z.-K.C. helped with confocal images. L.Z. helped with histological experiments.

DECLARATION OF INTERESTS

The authors declare no competing interests.

SUPPLEMENTAL INFORMATION

Supplemental information can be found online at https://doi.org/10.1016/j.celrep.2024.114140.

Ascl1-NSC pool. These findings suggest that sex-specific expression of distinct 5HTRs and their differential interactions with stress may underlie sex differences in stress vulnerability.

In brief

Luo et al. report sex-specific expression of distinct 5HTRs in adult mouse neural stem cells (NSCs) and their differential interaction with stress in regulating NSCs. Specifically, stress upregulates 5HT7Rs in NSCs of females and reduces the NSC pool via 5HT1ARs, while it downregulates 5HT7Rs in NSCs of males and maintains the NSC pool.

Graphical abstract

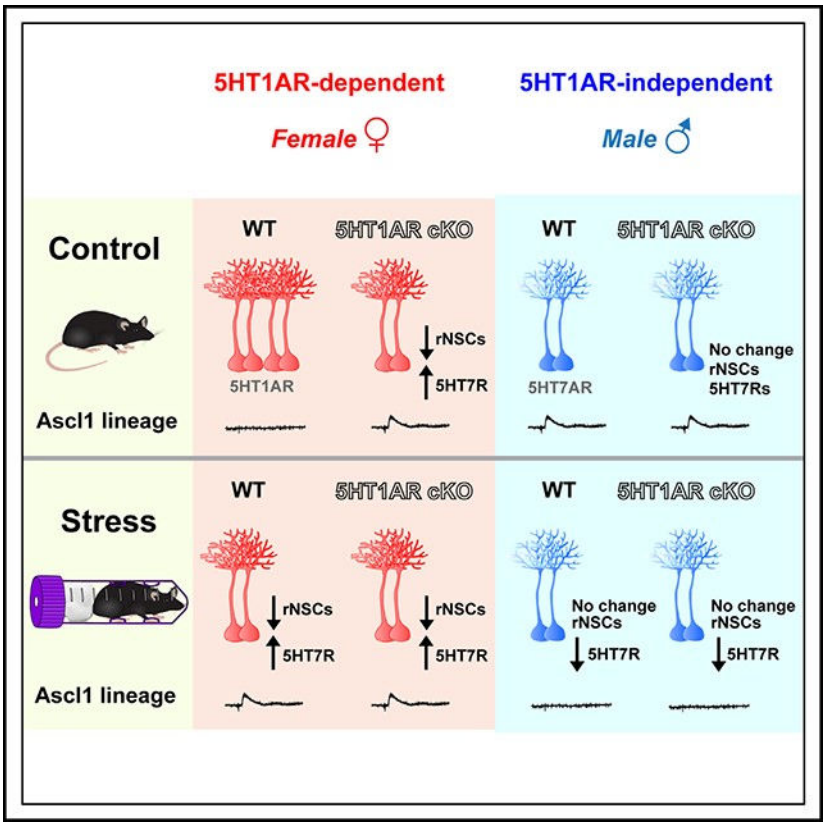

INTRODUCTION

The serotonin (5HT) system has been widely implicated in the pathophysiology of stress disorders, such as anxiety and depression.[1–3] Importantly, women are more vulnerable to stress, as reflected by a higher likelihood of developing these disorders in response to chronic stress.[4,5] These findings support the potential sex differences in the 5HT system, which may underlie sex-dependent responses to stress. The sex-dependent mechanisms underlying these outcomes remain poorly understood, as female subjects have historically been underrepresented in research associated with stress disorders.

The hippocampus is highly implicated in stress vulnerability and emotion regulation. One of the mechanisms that could account for alterations of hippocampal structure and function in response to chronic stress is the regulation of adult hippocampal neurogenesis, a process of generating new neurons from radial neural stem cells (rNSCs) in the adult dentate gyrus (DG). Accumulating evidence has shown that stress can alter the 5HT system and influence adult hippocampal neurogenesis in a sex-dependent manner.[6–11] Currently, we have a limited understanding of the mechanisms underlying sex differences in serotonergic regulation of adult hippocampal neurogenesis both at the baseline condition and in the context of stress. This is largely due to lack of information on the sex-dependent expression profile of 5HT receptors (5HTRs) in the neurogenic lineage and how stress interacts with distinct 5HTRs to regulate the neurogenic process.

Identification of cell-type-specific expression of 5HTRs is fundamentally important but extremely challenging because all seven classes of 5HTRs (a total of 14 subtypes) have been shown to be expressed in the hippocampus.[12,13] Among these 5HTRs, 5HT1A receptors (5HT1ARs) are the most studied 5HTR subtype in the contexts of stress responses, depression, antidepressant efficacy, and adult hippocampal neurogenesis regulation.[14–22] Specifically, previous studies have shown that systemic administration of 5HT1AR antagonists or agonists decreases or increases the number of proliferating cells, respectively, suggesting a critical role of 5HT1ARs in regulating proliferation of adult neural progenitors.[23–25] However, these studies used systemic drug manipulation, so it remains unknown whether these effects on neurogenesis are through a direct or indirect 5HT1AR-mediated signaling mechanism, as multiple types of dentate niche cells have been shown to express 5HT1ARs, such as dentate granule cells and local interneurons.[13] Moreover, they have primarily used thymidine analogs to study neurogenesis, thus biasing findings toward highly proliferative intermediate progenitors. Therefore, it remains unknown whether slowly proliferating rNSCs are subject to direct serotonergic regulation. Furthermore, sex differences in 5HT1ARs have been reported in both humans[26] and rodents.[27] However, it remains unknown whether expression of 5HT1ARs in adult rNSCs is sex dependent, and if so, whether this contributes to sex differences in rNSC regulation and whether stress interacts with sex-dependent expression of 5HT1ARs to differentially impact rNSC function across sexes.

In this study, we attempt to address these questions by selectively deleting 5HT1ARs in rNSCs derived from the Ascl1 lineage using mice from both sexes at baseline and under repeated restraint stress. Using a combination of slice electrophysiology, RNAscope, and *in vivo* fate mapping, we report sex-dependent receptor mechanisms underlying serotonergic regulation and stress vulnerability of adult hippocampal rNSCs. These findings not only fill the knowledge gap regarding sex-dependent serotonergic regulation of adult hippocampal neurogenesis, but also provide insights into the mechanisms underlying sex differences in stress vulnerability.

RESULTS

Selective deletion of 5HT1ARs in adult rNSCs decreases the rNSC pool in females

Recent single-cell RNA sequencing (scRNA-seq) of dentate Nestin-GFP+ cells has shown that 5HT1ARs, among all 5HTR subtypes, are the most abundant 5HTR subtype in neural stem/progenitor cells.[28] We sought to address the functional role of 5HT1ARs in regulating adult rNSC behaviors *in vivo* (Figure 1A). Recent studies using scRNA-seq and intravital imaging have revealed the existence of heterogeneous rNSC populations with distinct functional properties.[29,30] In this study, we focused on the Ascl1-rNSCs in the adult DG, an essential population of NSCs that exhibit initial short-term self-renewal followed by neurogenic proliferation prior to differentiation.[30] Toward this direction, we generated double-transgenic Ascl1-Ai9 mice as controls by crossing a tamoxifen (TMX)-inducible Ascl1-CreER^{T2} line[31] and a Cre-dependent floxed Ai9 reporter line expressing tdTomato,[32] referred to as wild-type (WT) mice, as well as triple-transgenic conditional knockout mice with selective deletion of 5HT1ARs in Ascl1-rNSCs, referred to as 5HT1AR cKO mice (Figure 1C). Given that we focus on the early lineage progression of Ascl1-rNSCs, we performed a relatively short lineage tracing of Ascl1-rNSCs and sacrificed animals 8 days post TMX induction (dpi) in WT and 5HT1AR cKO mice to capture the dynamics of Ascl1-rNSC maintenance (Figure 1B). Unexpectedly, we found sex differences in the total number of rNSCs following selective deletion of 5HT1ARs in adult Ascl1-rNSCs. Specifically, 5HT1AR cKO females exhibited a significant decrease in the number of Sox2+ GFAP+ tdTomato+ rNSCs (Figures 1D and 1F) as compared to WT female controls. In addition, 5HT1AR-mediated effects on rNSCs of females showed no significant differences between the dorsal and ventral DG (Figure 1G). By contrast, no significant difference in the total number of rNSCs was observed in males (Figures 1E and 1H). Notably, the labeling of tdTomato+ rNSCs in males was significantly lower than that in females. To address whether sex differences exist in adult rNSCs in these mice, we quantified the number of overall GFAP+ Sox2+ rNSCs (independent of Ai9-tdTomato expression) using the tissues from WT control mice. As a result, we found a non-significant decrease in the number of rNSCs in males as compared to females (Figures S1A and S1B). Therefore, these results do not fully explain the significant difference observed in tdTomato+ labeling between males and females. We speculate that the observed sex difference in tdTomato labeling in rNSCs might in part attibute to sex differences in TMX sensitivity. Such a difference has also been observed in other TMX-inducible lines labeling the neurogenic lineage from us and others (unpublished data). Therefore, to further validate sex-dependent effects mediated by 5HT1ARs, we normalized the number of tdTomato+ rNSCs in 5HT1AR cKO mice to the average number of their WT controls and compared these normalized values between males and females. As a result, we found significant sex differences (Figure 1I), thus supporting the sex-dependent role of 5HT1ARs in regulating the Ascl1-rNSC pool.

We next asked whether the decreased number of Ascl1-rNSCs in 5HT1AR cKO females was due to reduced proliferation by quantifying the number of Ki67+ Sox2+ GFAP+ tdTomato+ proliferating rNSCs in WT and 5HT1AR cKO females. No significant difference was observed in the number of proliferating rNSCs between WT and 5HT1AR cKO females (Figures S2A and S2B), suggesting that reduced rNSCs do not result from decreased

proliferation of rNSCs. The reduced rNSC pool could be due to reduced symmetric self-renewal of rNSCs, which might not be captured by proliferation markers due to the quiescent nature of rNSCs. To test this possibility, we performed clonal analysis with one dose of TMX to sparsely label Ascl1-rNSCs in WT and 5HT1AR cKO females (Figures S2C). As a result, no significant differences in symmetric self-renewal (clones containing two or more rNSCs) were found between WT control and 5HT1AR cKO females (Figures S2D and S2E). Together, these results suggest that the reduced Ascl1-rNSC pool in 5HT1AR cKO females likely results from precocious differentiation (not proliferation or symmetric self-renewal) of rNSCs. These results suggest a role of 5HT1ARs in rNSC maintenance by preventing precocious differentiation of Ascl1-rNSCs.

Adult rNSCs in females express 5HT1ARs

Next, we performed RNAscope in situ hybridization in combination with immunostaining to validate the 5HT1AR expression in neural stem/progenitors using nestin-GFP females. Within the hippocampus, the most abundant expression of Htr1a mRNA was found in CA1 pyramidal cells, followed by DG granule cells (Figure 2A), consistent with previous reports for the localization of 5HT1ARs.[13] Upon close examination of the subgranular zone, we found a subset of Nestin-GFP+ rNSCs (24 of 39, 61.5%) expressing Htr1a transcripts (Figure 2B).

As sex differences in 5HT1AR expression have been reported in both humans and rodents, we wondered whether the expression of 5HT1ARs in Ascl1-rNSCs is sex dependent. To address this question, we obtained a Cre-inducible gene trap reporter mouse line in which a variant of yellow fluorescent protein, YPet, is expressed under the control of the endogenous 5HT1AR promoter upon TMX administration (YPet mice).[20] To examine the level of 5HT1AR expression in rNSCs, we generated triple-transgenic mice by crossing YPet mice with Ascl1-Ai9 mice, referred to as Ascl1-YPet-Ai9 mice (Figures 2C and 2D). The purpose of incorporating Ai9 reporter is to use tdTomato fluorescence as a reference channel for YPet expression. We examined expression of YPet (immunopositive for GFP) and tdTomato in rNSCs by measuring the fluorescence intensities of GFP and tdTomato from both males and females at 8 dpi. The tdTomato and YPet fluorescence intensities were measured for each individual cell. Interestingly, tdTomato+ rNSCs in females exhibited a significantly higher level of GFP than tdTomato+ rNSCs in males (Figures 2E–2G), while the fluorescence intensity of tdTomato+ in rNSCs was similar between males and females (Figures 2E, 2F, and 2H). We also quantified the YPet/tdTomato ratio and found a significantly higher ratio in rNSCs of females than males (Figure 2I). These data suggested that Ascl1-rNSCs in females expressed a higher level of 5HT1ARs than males.

Deleting 5HT1ARs in rNSCs of females leads to upregulation of 5HT7Rs

Adult rNSCs do not have synapses, so the membrane potential (Vm) of these non-excitable cells has been established as an important readout for their cellular behavior.[33] Furthermore, our recent studies have established a correlation between the Vm and the rNSC behaviors *in vivo*.[34–36] Based on the role of 5HT1ARs in regulating rNSCs of females, we asked whether 5HT1ARs modulate the Vm of adult rNSCs in females. We recorded rNSCs at 8 dpi in WT and 5HT1AR cKO females upon bath application of 5HT in the presence of

tetrodotoxin (TTX) in order to block action potential-induced synaptic release from various DG niche cells (Figures 3A and 3B). The rNSCs were characterized by their distinct radial morphology, hyperpolarized Vm, and low input resistance (Figures S3A and S3B). In WT females, the mean Vm of rNSCs remained hyperpolarized in response to 5HT (Figures 3C and 3E). By contrast, in 5HT1AR cKO females, rNSCs exhibited 5HT-induced Vm depolarization (ranging from 14 to 59 mV, depolarization cutoff > 3 mV) (Figures 3D and 3E). Together, these data supported a role of 5HT1ARs for maintaining an inhibitory tone in rNSCs of females to prevent 5HT-induced depolarization.

5HT-induced depolarization in rNSCs of females with 5HT1AR deletion could be explained by (1) 5HT1AR deletion leading to upregulation of 5HT-depolarizing 5HTRs that are not normally present at a high level in rNSCs at baseline or (2) 5HT1AR deletion uncovering existing 5HT-depolarizing 5HTRs that are otherwise masked by the presence of 5HT1ARs. The second possibility can be tested by recording the Vm of rNSCs in the presence of the 5HT1AR antagonist spiroxatrine. We found that the Vm of rNSCs remained hyperpolarized upon bath application of 5HT (Figure 3E). These results suggested that 5HT1AR deletion induces upregulation of 5HTRs that are depolarizing to 5HT in Ascl1-rNSCs of females, as pharmacological blockade of 5HT1ARs did not uncover these 5HTRs in Ascl1-rNSCs.

We then sought to address the potential 5HTRs that are depolarizing to 5HT in Ascl1-rNSCs of females with 5HT1AR deletion. Recent studies have shown that 5HT1ARs and 5HT7Rs are co-expressed in the hippocampus, and their interplay has been implicated in mood disorders.[37] Moreover, activation of 5HT7Rs has been shown to exert slow depolarizing effects on hippocampal neurons.[38] Therefore, we tested the potential involvement of 5HT7Rs in mediating membrane depolarization of rNSCs in 5HT1AR cKO females. We recorded the Vm of rNSCs in 5HT1AR cKO females, followed by bath application of a selective 5HT7R antagonist, SB-269970, once 5HT-induced depolarization was observed. 5HT-induced Vm depolarization in rNSCs of 5HT1AR cKO females was abolished by bath application of SB-269970 (Figures 3F and 3G). These results suggest that deleting 5HT1ARs in Ascl1-rNSCs of females leads to 5HT-induced aberrant depolarization through upregulation of 5HT7Rs.

To further confirm the expression of these 5HTRs in rNSCs, we performed RNAscope of 5HT1AR and 5HT7R in Ascl1-rNSCs using WT and 5HT1AR cKO females. Consistent with the 5HT1AR expression in rNSCs of females, we found localization of Htr1a mRNA in rNSCs of WT mice, which was absent in rNSCs of 5HT1AR cKO mice (Figures 3H and 3I). By contrast, the localization of Htr7 mRNA in Ascl1-rNSCs of WT females was largely absent, but its localization was identified in Ascl1-rNSCs of 5HT1AR cKO females (Figures 3H and 3I). Therefore, these results confirmed our findings from slice electrophysiology.

Adult rNSCs in males express 5HT7Rs

Given that rNSCs in males express low-level 5HT1ARs, we wondered whether rNSCs of males express other types of 5HTRs. To approach this question, we first examined whether and how rNSCs in males respond to 5HT by recording the Vm of rNSCs. Unexpectedly, we observed 5HT-induced Vm depolarization in rNSCs (ranging from 8 to 51 mV) (Figures 4A and 4C), suggesting that a subset of rNSCs in males expresses 5HT-depolarizing 5HTRs.

We then investigated the potential 5HTR subtypes that are depolarizing to 5HT in rNSCs of males. We first confirmed the presence of 5HT7Rs in rNSCs by recording rNSCs in the presence of the 5HT7R antagonist SB-269970. As a result, a significant reduction in the magnitude of 5HT-induced depolarization was observed as compared to that recorded in the absence of SB-269970 (Figures 4B and 4C). To provide direct evidence of the presence of 5HT7Rs in rNSCs, we then recorded the Vm of the rNSCs upon spike application of 8-Hydroxy-2-(di-n-propylamino) tetralin (8-OH-DPAT), an agonist for both 5HT1ARs and 5HT7Rs, in the presence of both TTX and the 5HT1AR antagonist spiroxatrine to isolate the 5HT7R component. We found 8-OH-DPAT-induced Vm depolarization in rNSCs (ranging from 5 to 31 mV) (Figures 4D and 4E). Together, these results support the expression of 5HT7Rs in rNSCs of males as opposed to the expression of 5HT1ARs in rNSCs of females.

To further confirm the expression of these 5HT7Rs in rNSCs of males, we performed RNAscope of 5HT1AR and 5HT7R in Ascl1-rNSCs using WT male mice. Consistent with the 5HT7R expression in rNSCs of males, we found the localization of Htr7 mRNA in Ascl1-rNSCs (Figure 4G). By contrast, the localization of Htr1a mRNA in the rNSCs of male mice was largely missing (Figure 4F). Therefore, these results confirmed our findings from slice electrophysiology.

5HT1ARs mediate stress vulnerability of rNSCs in females

5HT1ARs have been widely implicated in stress response and anxiety/mood disorders, so we wondered whether stress interacts with 5HT1ARs to regulate rNSCs in a sex-dependent manner. Given that rNSCs in females express higher levels of 5HT1ARs, we asked whether stress selectively interacts with 5HT1ARs to regulate rNSCs in females. To address this, we subjected WT and 5HT1AR cKO females to a 4-day repeated restraint stress (RRS) paradigm (2 h/day at random times during the light cycle) or regular housing following TMX induction and examined RRS-induced effects on rNSCs in females (Figures 5A and 5B). The rationale for choosing RRS is based on published work showing that RRS alters the brain 5HT system[39,40] and adult hippocampal neurogenesis.[41,42] We quantified the densities of total rNSCs (Sox2+ GFAP+ tdTomato+) and proliferating rNSCs (Ki67+ Sox2+ GFAP+ tdTomato+) in non-stressed and stressed WT and 5HT1AR cKO females. In WT females, we found a significant reduction in both total and proliferating rNSCs (Figures 5C, 5G, and 5H) in stressed females as compared to non-stressed controls. In 5HT1AR cKO females, no differences were observed in the densities of total and proliferating rNSCs when comparing stressed and non-stressed 5HT1AR cKO females (Figures 5E, 5G, and 5H). To further address whether RRS interacts with 5HT1ARs in females to regulate the Ascl1-rNSC pool, we compared these measurements in WT and 5HT1AR cKO females using two-way ANOVA. Interestingly, our analysis showed that stress interacts with 5HT1ARs in regulating the rNSC pool (interaction of stress and genotype: $p = 0.047$) but not rNSC proliferation (interaction of stress and genotype: $p = 0.32$). Instead, the difference observed in the number of proliferating rNSCs was explained mainly by the stress factor (not the genotype) (treatment: $p = 0.027$, genotype: $p = 0.15$). These results suggest that the RRS-induced decrease in rNSCs occurs through a 5HT1AR-mediated mechanism, while the RRS-induced decrease in rNSC proliferation is independent of 5HT1ARs. These results align with our

results showing that selective deletion of 5HT1ARs in Ascl1-rNSCs of females impairs the maintenance (but not proliferation) of rNSCs (Figures 1F, S2A, and S2B).

We also examined RRS-induced effects on rNSCs in 5HT1AR cKO males. Two-way ANOVA did not detect significant differences in any of the categories (treatment, genotype, and interaction) in males (Figures 5D, 5F, 5I, and 5J), suggesting that RRS does not interact with 5HT1ARs in males for rNSC regulation. Together, these results support sex-dependent interaction of stress and 5HT1ARs in regulating Ascl1-rNSCs. Specifically, stress selectively interacts with 5HT1ARs in females to regulate Ascl1-rNSC maintenance (but not proliferation).

Stress upregulates 5HT7Rs in adult rNSCs of females through 5HT1ARs

Due to the potential interaction between 5HT1ARs and 5HT7Rs identified earlier in Ascl1-rNSCs of females (Figure 3), we sought to address whether RRS induces altered 5HT7R expression in rNSCs of females. To address this question, we recorded the Vm of rNSCs in non-stressed and stressed WT females upon spike application of 8-OH-DPAT in the presence of TTX and the 5HT1AR antagonist spiroxatrine to isolate the 5HT7R component (Figure 6A). Interestingly, 8-OH-DPAT induced Vm depolarization in rNSCs of stressed (but not non-stressed) WT females (ranging from 4 to 46 mV) (Figures 6B and 6C). These results supported stress-induced upregulation of 5HT7Rs in rNSCs of females. To address whether stress-mediated upregulation of 5HT7Rs in rNSCs of females occurs through 5HT1ARs, we recorded the Vm of rNSCs in non-stressed and stressed 5HT1AR cKO females. As a result, 8-OH-DPAT induced membrane depolarization in a similar portion of rNSCs in non-stressed and stressed 5HT1AR cKO females (Figures 6D and 6E). These results further confirmed 5HT7R upregulation in Ascl1-rNSCs of 5HT1AR cKO females (identified from Figure 3) and suggested that 5HT1ARs mediate RRS-induced upregulation of 5HT7Rs in Ascl1-rNSCs of females.

Stress downregulates 5HT7Rs in adult rNSCs of males

Next, we recorded the Vm of Ascl1-rNSCs from stressed and non-stressed WT males upon spike application of 8-OH-DPAT in the presence of TTX and the 5HT1AR antagonist spiroxatrine to isolate the 5HT7R component, similar to the manipulation in females. Consistent with the expression of 5HT7Rs in rNSCs of males, we observed 8-OH-DPAT-induced Vm depolarization in rNSCs of non-stressed WT males (ranging from 5 to 31 mV). Interestingly, such responses were absent in rNSCs of stressed WT males (Figures 6F and 6G). These results supported RRS-induced downregulation of 5HT7Rs in Ascl1-rNSCs of males.

To address whether stress-mediated downregulation of 5HT7Rs in Ascl1-rNSCs of males occurs through 5HT1ARs, we recorded the Vm of rNSCs in non-stressed and stressed 5HT1AR cKO males. As a result, non-stressed 5HT1AR cKO males exhibited 8-OH-DPAT-induced Vm depolarization in rNSCs (ranging from 7 to 73 mV) (Figures 6H and 6I), similar to that in WT males. These results supported the low expression of 5HT1ARs in rNSCs of males. Interestingly, similar to stressed WT males, stressed 5HT1AR cKO males failed to show 8-OH-DPAT-induced Vm depolarization in rNSCs (Figures 6H and 6I). These

results suggested that stressed-induced downregulation of 5HT7Rs in Ascl1-rNSCs of males is independent of 5HT1ARs.

Taken together, these results revealed sex-dependent effects of RRS on 5HT7R expression in rNSCs. Specifically, RRS-induced 5HT7R upregulation in Ascl1-rNSCs of females through a 5HT1AR-dependent mechanism, while RRS-induced 5HT7R downregulation in Ascl1-rNSCs of males is independent of 5HT1ARs.

DISCUSSION

In this study, we revealed a sex-dependent mechanism underlying serotonergic regulation of adult rNSCs at baseline and under stress (Figure S4). Specifically, we identified a sex-dependent 5HTR system in Ascl1-rNSCs: rNSCs in females express 5HT1ARs, while rNSCs in males express 5HT7Rs. Our findings that rNSCs in males express low levels of 5HT1ARs were consistent with a recent study showing that adult-born cells in males start to express 5HT1ARs from the immature neuron stage.[20] Functionally, selective deletion of 5HT1ARs in adult Ascl1-rNSCs of females reduces the rNSC pool, suggesting a role of 5HT1ARs in maintaining rNSCs. Mechanistically, we demonstrated that selective deletion of 5HT1AR in Ascl1-rNSCs of females leads to 5HT-induced depolarization in rNSCs mediated by 5HT7R upregulation. Interestingly, RRS interacts with 5HT1ARs in females to upregulate 5HT7Rs in Ascl1-rNSCs, leading to impaired rNSC maintenance. By contrast, Ascl1-rNSCs in males express 5HT7Rs, thus making them vulnerable to aberrant 5HT7R-mediated signaling. However, males appear to develop adaptive strategies to keep the 5HT7R-mediated signaling low under stress. Specifically, under stress, males exhibited reduced expression of 5HT7Rs in Ascl1-rNSCs, thus preventing rNSC depletion. Therefore, despite males expressing 5HT7Rs in rNSCs, these receptors are downregulated under stress to maintain low-level 5HT7R signaling in rNSCs. Such sex-dependent expression of 5HTRs in adult Ascl1-rNSCs and their distinct responses to stress may serve as a general mechanism underlying sex-dependent vulnerability to stress.

The cell-autonomous role of 5HT7Rs in regulating rNSCs of males remains to be determined due to lack of floxed mouse lines for 5HT7Rs. Our studies showed that RRS reduced 5HT7R expression in rNSCs of males, which correlates with a non-significant increase in the number of Ascl1-rNSCs. These results suggest that stress-induced downregulation in 5HT7Rs and the subsequent decrease in 5HT7R-mediated signaling maybe beneficial for rNSC maintenance in males. Future studies via direct manipulation of 5HT7Rs in rNSCs of males will be able to address the causal role of 5HT7Rs in regulating rNSCs at baseline or under stress.

Our studies showed that selective deletion of 5HT1ARs in Ascl1-rNSCs of females induces 5HT-induced depolarization and impaired rNSC production. These results suggest that 5HT1ARs may provide an inhibitory tone that is crucial for Ascl1-rNSC maintenance in females. Furthermore, we showed that 5HT-induced depolarization in rNSCs of 5HT1AR cKO females is mediated by upregulation of 5HT7Rs, thus highlighting the interplay between 5HT1ARs and 5HT7Rs in rNSC regulation. The signaling mechanisms underlying the interplay between 5HT1ARs and 5HT7Rs in regulation of adult rNSCs remain

elusive. 5HT7Rs are canonically Gs-coupled receptors, and activation of the Gs family of proteins stimulates the production of the second messenger cyclic AMP (cAMP) by adenylyl cyclase (AC).[43] By contrast, 5HT1ARs are Gi/o-coupled receptors, and activation of the Gi/o family of proteins inhibits AC activity, decreasing cAMP levels.[44] The interplay of these two arms of cAMP signaling may be critical for regulating Vm and functions of rNSCs. Specifically, a 5HT1AR-mediated decrease of cAMP signaling may be critical for maintaining hyperpolarized Vm of rNSCs and supporting rNSC maintenance, while a 5HT7R-mediated increase of cAMP signaling may induce aberrant membrane depolarization of rNSCs and impair rNSC maintenance.

In this study, we speculate that reduced Ascl1-rNSC pool in 5HT1AR cKO females likely results from precocious differentiation of Ascl1-rNSCs. Differentiation of rNSCs could be accompanied by a transient increase of neural progenitors or astrocytes. To address this possibility, we examined the number of Sox2+ type 2a early neural progenitors thought to derive from rNSCs. However, we failed to observe increased type 2a cells in 5HT1AR cKO mice as compared to WT controls. We speculate that 5HT1ARs may regulate differentiation of both rNSCs and type 2a progenitors so that deletion of 5HT1ARs in rNSCs and type 2a progenitors led to both an increased number of type 2a progenitors (through precocious differentiation of rNSCs) and a decreased number of type 2a progenitors (through precocious differentiation of type 2a cells). Therefore, these opposing effects lead to an unaltered number of type 2a cells. Furthermore, we examined Sox2-negative intermediate progenitors and observed significant decrease in this population along with significantly decreased proliferation of this population (Figures S5A and S5B), with no changes in males (Figures S5C and S5D). These results suggest that 5HT1ARs are required for regulating proliferation of intermediate progenitors in females, and this effect likely overrides the effects of increased differentiation of rNSCs/type 2a progenitors. In addition, we also examined the rNSC clones to see if we could identify transitioning rNSCs that are in the process of differentiating into astrocytes[45] but failed to observe an increased occurrence of transitioning rNSCs. These results support the critical role of 5HT1ARs in regulating neuronal lineage in females.

Adult hippocampal neurogenesis is highly sensitive to stress and glucocorticoids.[11] It has been shown that ablation of adult hippocampal neurogenesis causally correlates with increased corticosterone levels and impaired stress reactivity in response to RRS.[46] In addition, RRS alters 5HT1AR expression in a sex-dependent fashion with decreased 5HT1AR mRNA expression in the hippocampus of female (but not male) rats.[47] These results, along with our findings that RRS decreases the number of neural precursors in a 5HT1AR-dependent manner only in female mice, collectively support a sex-dependent role of 5HT1ARs in regulating hippocampal function in response to stress. Such a 5HT1AR-dependent, female-specific reduction in adult rNSCs and hippocampal neurogenesis may predispose females to enhanced responses to future stress and development of depressive behaviors. Human studies have shown that women are more likely to suffer from stress-induced mood disorders, such as anxiety and depression.[4,5] Therefore, our study provides an entry point toward a better understanding of the sex differences associated with these disorders. Ultimately, such information will enable development of personalized strategies to treat these detrimental conditions.

Limitations of the study

It remains to be determined whether the overall rNSC pool changes in 5HT1AR cKO females. Ascl1-rNSCs represent a specific subpopulation of rNSCs,[29] thus making it challenging to assess the overall rNSC pool with the manipulation of 5HT1ARs only in this subpopulation. Additionally, it remains to be determined whether 5HTR-mediated mechanisms also apply to other rNSC populations, such as Nestin/Gli1-rNSCs. Future studies using different rNSC-labeling CreER lines (i.e., Nestin/Gli1-CreER) in combination with a floxed 5HT1AR mouse line would be able to address this question.

STAR★METHODS

RESOURCE AVAILABILITY

Lead contact—Further information and requests for resources and reagents should be directed to and will be fulfilled by the lead contact, Juan Song (juansong@email.unc.edu).

Materials availability—This study did not generate new unique reagents.

Data and code availability

- All data reported in this paper will be shared by the lead contact upon request.
- This paper does not report original code.
- Any additional information required to reanalyze the data reported in this paper is available from the lead contact upon request.

EXPERIMENTAL MODEL AND STUDY PARTICIPANT DETAILS

Animals—The following adult mice (7–11 week, males and females) were used in this study: Nestin-GFP,[49] Ai9 (JAX stock #007909), Ascl1-CreER (JAX stock #012882), floxed 5HT1AR[48] (generous gift from Dr. Thomas Kash at UNC), and floxed 5HT1A-YPet mice (generous gift from Dr. Rene Hen at Columbia University[20]), and C57BL/6J mice (JAX stock #000664). All the mouse lines in this study are on the C57BL/6J background. For quantification of 5HT1AR expression, floxed YPet (fL/fL) males were crossed with Ascl1-CreER (+/−) Ai9 (fL/fL) females to generate triple transgenic Ascl1-CreER (+/−) Ai9 (fl/+) YPet (fl/+) mice, referred to as Ascl1-YPet-Ai9 mice. For lineage tracing, Ascl1-CreER (+/−) males were crossed with Ai9 (fL/fL) females to generate double transgenic Ascl1-CreER (+/−) Ai9 (fl/+) mice as control mice (referred to as WT mice). 5HT1AR (fL/fL) males were crossed with Ai9(fl/fl) Ascl1-CreER (+/−) 5HT1AR (fL/fL) females to generate triple transgenic Ascl1-CreER (+/) Ai9 (fl/+) 5HT1AR (fL/fL) mice with selective deletion of 5HT1ARs in the Ascl1+ neurogenic lineage as experimental mice (referred to as 5HT1AR cKO mice). Animals were separated by sex at weaning and group housed with 3–5 animals per cage. Mice up to 10 days of age were toe-clipped for genotyping. Only virgin animals were used for experiments. Littermates of the same sex were randomly assigned to experimental groups. All mice were fed on standard diets in standard ventilated cages (13 × 6” floor space) with the 12/12 light-dark cycle (light from 7:00 a.m. to 7:00 p.m.). Animal procedures were conducted in accordance with the guide for the Care and Use of Laboratory

Animals, as adopted by the NIH, and with approval of the Institutional Animal Care and Use Committee at the University of North Carolina at Chapel Hill.

METHOD DETAILS

Tamoxifen induction—Tamoxifen (Sigma-aldrich T5648) was dissolved in corn oil (1 mg/50 μL) at 55° for 15 min with vortexing and aliquots were stored in a −20°C freezer, and aliquots were used within 60 days. At 8–11 week of age (median age: postnatal day 66; average age: 67 ± 6.5 days standard deviation), mice received an intraperitoneal (ip) injection of tamoxifen at 80 mg/kg on two consecutive days to induce Cre recombination activity. Typically, females (median weight: 18 g; average: 18.12 ± 1.5 g) weighed less than males (median weight: 23 g; average: 22.55 ± 2.4 g) and received on average 20% less injection volume (~100 μL males, ~80 μL females). Mice were returned to their home cage after injection and animal's general health was monitored daily.

Repeated restraint stress—For *in vivo* lineage tracing experiments using restraint stress, animals were given tamoxifen and then allowed to remain in their home cage without intervention for 48 h. The animals were brought to a satellite facility within the same building and subjected to 4 repeated days of restraint stress from day 4–7. On day 8, mice were sacrificed. Restraint stress was applied by scruffing the mice and inserting them into modified 50 mL conical tubes (6 × 4mm air holes were made by manual drilling through the plastic) and placing the restrained mouse in a new cage with clean bedding for 2 h. At the end of 2 h, the mice were released back into their homecage. Conical tubes were cleaned with hot soapy water and reused the next day. Animals were unable to turn around when restrained. For *in vitro* electrophysiology studies, 5HT1AR cKO and WT mice of both sexes were given tamoxifen on the first 2 days and then were restrained for 2 h per day for 4 consecutive days (from day 4 to day 7), and stressed mice were used for recording immediately after the last restraint.

Immunohistochemistry (IHC)—Fixed brain samples were collected by transcardial perfusion. Briefly mice were terminally exposed to a lethal dose of isoflurane in an incubation chamber. At the cessation of breathing, the chest cavity was exposed and a 27G needle was inserted into the left ventricle and PBS (~15 mL) was first flowed by a peristaltic pump, followed by 4% formaldehyde (PFA, ~20 mL) in PBS within the same line. Brains were extracted and post fixed in 4% PFA overnight, cryoprotection and dehydration in 30% sucrose for 48 h. Coronal sections were cut using a freezing sliding microtome (Leica) at 60 μm thickness and processed for immunostaining. Sections designated for free floating antibody staining went through pretreatment steps as following; 3 × 5-min incubations in 1 mg/mL Sodium borohydride in PBS, then 2 × 1 h incubations in 0.3% Triton X- in PBS. A blocking step was then performed using 5% donkey serum in 0.1% PBST. Sections were then transferred to the primary antibody solution in 0.1% PBST with 3% donkey serum and kept at 40° for 2 days. Information on the manufactures of antibodies can be found in the key resources table. Primary antibodies were applied in the following concentrations: anti-GFP (goat, 1:500), anti-Ki67 (rabbit, 1:500), anti-Sox2 (goat, 1:400), and anti-GFAP (mouse, 1:1000). Following 3 × 10-min washing in PBS, sections were transferred to secondary antibodies (all: 1:800) in 0.1% PBST for 16–24 h at 4°. After washing, sections

were incubated with DAPI, washed with PBS, and coverslipped with Diamond prolong gold mounting media (Thermo Fisher Scientific, P36961).

For biocytin staining after whole-cell patch-clamp recording, tissues containing biocytin-loaded cells were fixed in 4% PFA. After washing, slices were incubated in PBST containing streptavidin conjugated to Alexa 647 (1:1000; Invitrogen Molecular Probes, USA) and DAPI (1:500; Thermo fisher scientific, USA) for 12-h at 4°.

***In situ* hybridization (ISH)—**For Nestin-GFP mice, mouse brains were embedded in OCT (Sakura) immediately after fixation and sucrose equilibration and cut in 10-μm thick sections of the hippocampus on a cryostat. The sections were collected on glass slides and ISH was performed using the RNA-Scope 2.5 HD Reagent Kit-RED (cat#322350). Dual ISH-IHC was carried out according to manufacturer's instructions (Advanced Cell Diagnostics). Briefly, sections were baked onto glass slides and were exposed to H_2O_2 then heat antigen retrieval (using citrate buffer) followed by 30 min protease pretreatment steps. For ISH labeling, we used Htr1a Probe - Mm-Htr1a (cat#312301) or Negative Control Probe - DapB (cat#310043). The detection of the 5HT1a receptor transcript was combined with standard immunofluorescence for GFP, and DAPI staining to visualize the nuclei. GFP staining was done immediately after ISH and Goat GFP primary antibody (Rockland) and anti-Goat Alexa 488 secondary were used. Finally, sections were mounted in EcoMount according to manufacturer's protocol (Advanced Cell Diagnostics).

For Ascl1-Ai9 WT mice and Ascl1–5HT1AR-Ai9 conditional knockout (5HT1AR cKO) mice, both sexes were used for ISH staining. Mice were perfused at 7 days after Tamoxifen injections. After fixation and sucrose equilibration, mouse brains were embedded in OCT (Sakura) and cut in 15-μm thick sections of the hippocampus on a cryostat. The sections were collected on glass slides and ISH was performed using the RNA-Scope Fluorescent Multiplex V2 Kit (cat#323110). UNC Pathology core performed this staining procedure. Dual ISH-IHC was carried out according to manufacturer's instructions (Advanced Cell Diagnostics). Briefly, sections were exposed to H_2O_2 then heat antigen retrieval and followed by a 5 min protease pretreatment step. For ISH labeling, we used Mm-Htr7 Probe (Cat#401321) and Htr1a Probe - Mm-Htr1a (cat#312301-C2), and detected with cy5. Additional IHC was performed with staining for tdtomato (Rabbit dsRed primary antibody, 1:500, Takara Cat#632496), and detected with goat anti-rabbit Alexa Fluor 488 (1:1000, Invitrogen #A32731). Finally, sections were coverslipped using Fluorogel II with DAPI (Electron Microscopy Sciences #17985–50).

Clonal lineage analysis—Clonal analysis was conducted in Ascl1–5HT1AR-Ai9 conditional knockout (5HT1AR cKO) female mice and Ascl1-Ai9 controls with sparse labeling by injecting one dose of 80 mg/kg tamoxifen. Mice were perfused at 7 days post tamoxifen injection. Serial sections (60 μm thickness) from left and right hemispheres were collected separately and were stained for DAPI. Images acquisition and analysis were restricted to entire dentate gyrus along the dorsal-ventral axis. TdTomato+ Ascl1-rNSCs were classified for symmetric or asymmetric cell divisions based upon the morphology of individual cells within a clone, similar to the approach described in.[45,51] Images were acquired using an Olympus FV3000 confocal microscope as 30–35 Z-stacks with a step size

of 1.0 μm. Mice with less than 2 clones per hemisection on average were determined as standard for sparse labeling and were selected for clonal analysis.

Imaging—Confocal imaging was performed using an Olympus FV3000 system. A 20X/0.75 U Plan S-Apo objective was used for lineage tracing data, YPet quantification and biocytin staining cells. A 40X/1.3 UPLXAPO oil objective was used for clonal analysis quantification. Image resolution varied by experimental needs. Resolution ranged from 0.15–0.75 μm in XY pixel size and ranged from 0.3–1 μm in axial step.

Quantification—All imaging and quantification were performed blind to the experimental group.

For YPet quantification, only Ai9 cells located along SGZ and with typical radial process were identified as rNSC. ROIs were manually defined around the soma of the rNSC with ROI manager in ImageJ. Intensity of both YPet and tdTomato values of each individual cell were measured and exported for further analysis.

To quantify Htr1a mRNA in Nestin-GFP+ rNSCs, manual counting of the probe labeling was performed in ImageJ. If GFP+ cells exhibit colocalization with the probes, they will be scored as Htr1a positive cells (GFP+ cells usually have 1–3 puncta per cell); if no puncta were found, they will be scored as Htr1a negative cells.

For quantification of tdTomato+ cells along with specific cellular markers, serial brain sections were processed by IHC for Ki67, Sox2, and GFAP. Sox2 and GFAP were stained in the far-red channel by using a mix of Alexa 647 secondaries of both species, as described in our recent publication.[36] These two markers can be distinguished as Sox2 is exclusively nuclear, whereas GFAP was exclusively cytoplasmic. rNSCs are characterized by molecular marker expression and morphology. Specifically, typical rNSCs exhibit GFAP+ radial processes and are Sox2+. For stereological counting, we followed an optical fractionator sampling scheme as previously described by Encinas et al.,[49] and we have used similar approaches with minor modifications in a number of our previous studies.[34–36,51–54] Specifically, coronal sections through the entire DG (from −1.55 mm to −3.39 mm to bregma) were collected in a serial order using 48-well plates. The 50 μm slices were collected in 8 parallel sets, and each set consists 6 slices along the dorsoventral axis. We randomly selected a set of 6 slices along the dorsoventral axis of DG (each slice ~400 μm apart from the next) to take into account of the entire DG structure. For counting in dorsal and ventral DG separately, the following coordinates were used: dorsal DG (bregma −1.55 mm to bregma −2.27 mm) and ventral DG (bregma −2.79 mm to bregma −3.39 mm). All rNSCs positive for tdTomato or combined tdTomato and other cellular markers (Sox2, GFAP, or Ki67) were counted to obtain absolute cell numbers from a set of 6 slices using the Cell Counter plugin in ImageJ. The volume of DG was calculated through multiplying the area of the SGZ+GCL by the thickness of the slice. For each animal, the total cell number was calculated by normalizing the absolute number of tdTomato+ cells to the DG volume.

Ex vivo patch-clamp electrophysiology

Preparation of acute brain slices: Nestin-GFP mice, Ascl1-Ai9 double transgenic mice and triple transgenic (5HT1AR cKO) mice of both sexes, 8–10 weeks old were used for experiments. Animals were deeply anesthetized with isoflurane, perfused intra-cardially with oxygenated ice-cold NMDG solution containing (in mM).[34] 92 NMDG, 30 $NaHCO_3$, 25 glucose, 20 HEPES, 10 $MgSO_4$, 5 sodium ascorbate, 3 sodium pyruvate, 2.5 KCl, 2 thiourea, 1.25 NaH2PO_4, 0.5 $CaCl_2$ (pH 7.3, 310 mOsm). The brain was removed quickly and placed in additional ice-cold NMDG solution for slicing. Transverse hippocampal slices (280 μm thick) were prepared using a Leica VT1200S vibratome and warmed to 34.5°C for 8 min. The slices were subsequently maintained in the HEPES holding solution containing (in mM): 92 NaCl, 30 $NaHCO_3$, 25 glucose, 20 HEPES, 5 sodium ascorbate, 3 sodium pyruvate, 2.5 KCl, 2 thiourea, 2 $MgSO_4$, 2 $CaCl_2$, 1.25 NaH_2PO_4 (pH 7.3, 310 mOsm) at room temperature for at least 1 h.

Electrophysiological recordings were made at 32°C using a heater controller (TC-324C, Warner Instruments) in artificial cerebrospinal fluid (ACSF) containing (in mM): 125 NaCl, 26 $NaHCO_3$, 20 glucose, 2.5 KCl, 2 $CaCl_2$, 1.3 $MgSO_4$, 1.25 NaH2PO4, (pH 7.3, 310 mOsm). The flow rate was 2 mL/min. GFP+ or Ai9+ neurons within the sub-granule zone were visualized by differential interference contrast (DIC) and fluorescence microscopy.

Patch-clamp recordings—Patch pipettes with a resistance of 4–6 MΩ were pulled from borosilicate glass capillaries (1.5/0.84 mm, World Precision Instruments) using a micropipette puller (PC-10, Narishige, Japan). The pipettes were filled with an internal solution containing the following (in mM): 130 K-gluconate, 20 HEPES, 4 $MgCl_2$, 4 Na-ATP, 2 NaCl, 0.5 EGTA, 0.4 Na-GTP (pH 7.2, 290–300 mOsm). In some experiments, 0.1% biocytin (v/v, Sigma, USA) was included in the internal solution. Recordings were conducted in the whole-cell configuration using a Multiclamp 700B amplifier (Axon Instruments). Signals were filtered at 2 kHz and sampled at 10 kHz using the Digidata 1440A (Axon Instruments), data acquisition and pulse generation were performed using pClamp 10.7 (Axon Instruments). Series resistance (Rs) was monitored throughout all experiments and cells with Rs changes over 20% were discarded.

The drugs used include Serotonin hydrochloride (5HT), Spiroxatrine (spi), (±)-8-hydroxy-2-dipropylaminotetralin hydrobromide (8-OH-DPAT), tetrodotoxin (TTX), and SB-269970. All chemicals were obtained from Tocris and stored in stock solutions at −20°C and dissolved in fresh oxygenated ACSF to the final concentration immediately before each experiment. All drugs were applied by bath application except 8-OH-DPAT (10 mM concentration of 50 μL) was delivered by spike application using a pipette close to the patched cells. Pharmacological agents were used at the following final concentrations in the bath as indicated: 5HT (20 μM), TTX (1 μM), Spiroxatrine (spi, 1 μM), and SB-269970 (10 μM).

For quantification of electrophysiology data, we plot the data by cell numbers instead of animals due to generally low cell numbers recorded from individual animals (some animals only have 1–2 cells/animal). This is largely due to the low percentage of Ascl1-rNSCs (~18% out of total tdTomato+ cells) and technical challenges of patching rNSCs.

QUANTIFICATION AND STATISTICAL ANALYSIS

All data are reported as means or means ± SEM. Shapiro-Wilk test was performed for normality of all datasets. For the datasets with normal distribution, statistical analyses were preformed via two-tailed unpaired t test, and two-way repeated measures ANOVA followed by Sidak's multiple comparisons test. Two-tailed paired t-tests were applied to *in vitro* electrophysiology data. For the nonnormally distributed datasets, two-tailed Mann Whitney tests were performed. Contingency tables were analyzed by two-sided Fisher's exact test. All statistical methods, sample size and p-values were indicated in figure legends. Sample size number could represent animal number, cell number and slice number etc, details were described in the corresponding figure legends. Significance was defined as $*p < 0.05$, $**p < 0.01$, $***p < 0.001$. GraphPad Prism 8 software (San Diego, CA) was used for the analyses.

Supplementary Material

Refer to Web version on PubMed Central for supplementary material.

ACKNOWLEDGMENTS

We acknowledge members of the Song lab for comments and discussions. We acknowledge Dr. Rene Hen at Columbia University for sharing the YPet mice. We acknowledge Ashley J. Ezzell at the UNC Histology Core for the technical support of the RNA-Scope experiment. Confocal microscopy was performed at the UNC Neuroscience Microscopy Core Facility, supported in part by funding from NIH-NINDS Neuroscience Center Support Grant P30 NS045892 and NIH-NICHD Intellectual and Developmental Disabilities Research Center Support Grant U54 HD079124. This work was supported by grants awarded to J.S. from the NIH (RF1AG071000, R01MH122692, R01NS121300, R01AG084207, and R01MH132222). A.C. was partially supported by an NIHT32 predoctoral training grant, an NIH predoctoral fellowship (F31MH110146), and a UNC Dissertation Completion Fellowship. Y.-D.L. was partially supported by a NARSAD Young Investigator Award from the Brain & Behavior Research Foundation (29600).

REFERENCES

1. Chaouloff F (1993). Physiopharmacological interactions between stress hormones and central serotonergic systems. Brain research. Brain Res. Rev. 18, 1–32. [PubMed: 8467346]
2. Bach-Mizrachi H, Underwood MD, Tin A, Ellis SP, Mann JJ, and Arango V (2008). Elevated expression of tryptophan hydroxylase-2 mRNA at the neuronal level in the dorsal and median raphe nuclei of depressed suicides. Mol. Psychiatr. 13, 507–465. 10.1038/sj.mp.4002143.
3. Jacobsen JPR, Medvedev IO, and Caron MG (2012). The 5-HT deficiency theory of depression: perspectives from a naturalistic 5-HT deficiency model, the tryptophan hydroxylase 2Arg439His knockin mouse. Philos. Trans. R. Soc. Lond. B Biol. Sci. 367, 2444–2459. 10.1098/rstb.2012.0109. [PubMed: 22826344]
4. Brody DJ, Pratt LA, and Hughes JP (2018). Prevalence of Depression Among Adults Aged 20 and over: United States, 2013–2016 (NCHS data brief), pp. 1–8. [PubMed: 29638213]
5. Ferretti MT, Iulita MF, Cavedo E, Chiesa PA, Schumacher Dimech A, Santuccione Chadha A, Baracchi F, Girouard H, Misoch S, Giacobini E, et al. (2018). Sex differences in Alzheimer disease - the gateway to precision medicine. Nat. Rev. Neurol. 14, 457–469. 10.1038/s41582-018-0032-9. [PubMed: 29985474]
6. Hodes GE, Hill-Smith TE, Suckow RF, Cooper TB, and Lucki I (2010). Sex-specific effects of chronic fluoxetine treatment on neuroplasticity and pharmacokinetics in mice. J. Pharmacol. Exp. Therapeut. 332, 266–273. 10.1124/jpet.109.158717.
7. Yagi S, and Galea LAM (2019). Sex differences in hippocampal cognition and neurogenesis. Neuropsychopharmacology 44, 200–213. 10.1038/s41386-018-0208-4. [PubMed: 30214058]

8. Hillerer KM, Neumann ID, Couillard-Despres S, Aigner L, and Slattery DA (2013). Sex-dependent regulation of hippocampal neurogenesis under basal and chronic stress conditions in rats. Hippocampus 23, 476–487. 10.1002/hipo.22107. [PubMed: 23504963]
9. Falconer EM, and Galea LAM (2003). Sex differences in cell proliferation, cell death and defensive behavior following acute predator odor stress in adult rats. Brain Res. 975, 22–36. 10.1016/s0006-8993(03)02542-3. [PubMed: 12763590]
10. Westenbroek C, Den Boer JA, Veenhuis M, and Ter Horst GJ (2004). Chronic stress and social housing differentially affect neurogenesis in male and female rats. Brain Res. Bull. 64, 303–308. 10.1016/j.brainresbull.2004.08.006. [PubMed: 15561464]
11. Mirescu C, and Gould E (2006). Stress and adult neurogenesis. Hippocampus 16, 233–238. 10.1002/hipo.20155. [PubMed: 16411244]
12. Berumen LC, Rodríguez A, Miledi R, and García-Alcocer G (2012). Serotonin receptors in hippocampus. Sci. World J. 2012, 823493. 10.1100/2012/823493.
13. Tanaka KF, Samuels BA, and Hen R (2012). Serotonin receptor expression along the dorsal-ventral axis of mouse hippocampus. Philos. Trans. R. Soc. Lond. B Biol. Sci. 367, 2395–2401. 10.1098/rstb.2012.0038. [PubMed: 22826340]
14. Samuels BA, Mendez-David I, Faye C, David SA, Pierz KA, Gardier AM, Hen R, and David DJ (2016). Serotonin 1A and Serotonin 4 Receptors: Essential Mediators of the Neurogenic and Behavioral Actions of Antidepressants. Neuroscientist 22, 26–45. 10.1177/1073858414561303. [PubMed: 25488850]
15. Le Franç ois B, Czesak M, Steubl D, and Albert PR (2008). Transcriptional regulation at a HTR1A polymorphism associated with mental illness. Neuropharmacology 55, 977–985. 10.1016/j.neuropharm.2008.06.046. [PubMed: 18639564]
16. Strobel A, Gutknecht L, Rothe C, Reif A, Mössner R, Zeng Y, Brocke B, and Lesch KP (2003). Allelic variation in 5-HT1A receptor expression is associated with anxiety- and depression-related personality traits. J. Neural. Transm. 110, 1445–1453. 10.1007/s00702-003-0072-0. [PubMed: 14666415]
17. Garcia-Garcia AL, Newman-Tancredi A, and Leonardo ED (2014). 5-HT(1A) [corrected] receptors in mood and anxiety: recent insights into autoreceptor versus heteroreceptor function. Psychopharmacology (Berl) 231, 623–636. 10.1007/s00213-013-3389-x. [PubMed: 24337875]
18. Akimova E, Lanzenberger R, and Kasper S (2009). The serotonin-1A receptor in anxiety disorders. Biol. Psychiatr. 66, 627–635. 10.1016/j.biopsych.2009.03.012.
19. Szewczyk B, Kotarska K, Daigle M, Misztak P, Sowa-Kucma M, Rafalo A, Curzytek K, Kubera M, Basta-Kaim A, Nowak G, and Albert PR (2014). Stress-induced alterations in 5-HT1A receptor transcriptional modulators NUDR and Freud-1. Int. J. Neuropsychopharmacol. 17, 1763–1775. 10.1017/S146114571400100X.
20. Samuels BA, Anacker C, Hu A, Levinstein MR, Pickenhagen A, Tsetsenis T, Madroñal N, Donaldson ZR, Drew LJ, Dranovsky A, et al. (2015). 5-HT1A receptors on mature dentate gyrus granule cells are critical for the antidepressant response. Nat. Neurosci. 18, 1606–1616. 10.1038/nn.4116. [PubMed: 26389840]
21. Alenina N, and Klempin F (2015). The role of serotonin in adult hippocampal neurogenesis. Behav. Brain Res. 277, 49–57. 10.1016/j.bbr.2014.07.038. [PubMed: 25125239]
22. Santarelli L, Saxe M, Gross C, Surget A, Battaglia F, Dulawa S, Weisstaub N, Lee J, Duman R, Arancio O, et al. (2003). Requirement of hippocampal neurogenesis for the behavioral effects of antidepressants. Science 301, 805–809. 10.1126/science.1083328. [PubMed: 12907793]
23. Radley JJ, and Jacobs BL (2002). 5-HT1A receptor antagonist administration decreases cell proliferation in the dentate gyrus. Brain Res. 955, 264–267. [PubMed: 12419546]
24. Banasr M, Hery M, Printemps R, and Daszuta A (2004). Serotonin-induced increases in adult cell proliferation and neurogenesis are mediated through different and common 5-HT receptor subtypes in the dentate gyrus and the subventricular zone. Neuropsychopharmacology 29, 450–460. 10.1038/sj.npp.1300320. [PubMed: 14872203]
25. Mori M, Murata Y, Matsuo A, Takemoto T, and Mine K (2014). Chronic Treatment with the 5-HT1A Receptor Partial Agonist Tandospirone Increases Hippocampal Neurogenesis. Neurol. Ther. 3, 67–77. 10.1007/s40120-013-0015-0. [PubMed: 26000223]

26. Jovanovic H, Lundberg J, Karlsson P, Cerin A, Saijo T, Varrone A,Halldin C, and Nordström AL (2008). Sex differences in the serotonin 1A receptor and serotonin transporter binding in the human brain measured by PET. Neuroimage 39, 1408–1419. 10.1016/j.neuroimage.2007.10.016. [PubMed: 18036835]
27. Goodfellow NM, Benekareddy M, Vaidya VA, and Lambe EK (2009). Layer II/III of the prefrontal cortex: Inhibition by the serotonin 5-HT1A receptor in development and stress. J. Neurosci. 29, 10094–10103. 10.1523/JNEUROSCI.1960-09.2009. [PubMed: 19675243]
28. Shin J, Berg DA, Zhu Y, Shin JY, Song J, Bonaguidi MA, Enikolopov G, Nauen DW, Christian KM, Ming GL, and Song H (2015). Single-Cell RNA-Seq with Waterfall Reveals Molecular Cascades underlying Adult Neurogenesis. Cell Stem Cell 17, 360–372. 10.1016/j.stem.2015.07.013. [PubMed: 26299571]
29. Bottes S, Jaeger BN, Pilz GA, Jörg DJ, Cole JD, Kruse M, Harris L, Korobeynyk VI, Mallona I, Helmchen F, et al. (2021). Long-term self-renewing stem cells in the adult mouse hippocampus identified by intravital imaging. Nat. Neurosci. 24, 225–233. 10.1038/s41593-020-00759-4. [PubMed: 33349709]
30. Pilz GA, Bottes S, Betizeau M, Jörg DJ, Carta S, April S, Simons BD, Helmchen F, and Jessberger S (2018). Live imaging of neurogenesis in the adult mouse hippocampus. Science 359, 658–662. 10.1126/science.aao5056. [PubMed: 29439238]
31. Kim EJ, Leung CT, Reed RR, and Johnson JE (2007). In vivo analysis of Ascl1 defined progenitors reveals distinct developmental dynamics during adult neurogenesis and gliogenesis. J. Neurosci. 27, 12764–12774. 10.1523/JNEUROSCI.3178-07.2007. [PubMed: 18032648]
32. Madisen L, Zwingman TA, Sunkin SM, Oh SW, Zariwala HA, Gu H, Ng LL, Palmiter RD, Hawrylycz MJ, Jones AR, et al. (2010). A robust and high-throughput Cre reporting and characterization system for the whole mouse brain. Nat. Neurosci. 13, 133–140. 10.1038/nn.2467. [PubMed: 20023653]
33. Levin M (2014). Molecular bioelectricity: how endogenous voltage potentials control cell behavior and instruct pattern regulation in vivo. Mol. Biol. Cell 25, 3835–3850. 10.1091/mbc.E13-12-0708. [PubMed: 25425556]
34. Asrican B, Wooten J, Li YD, Quintanilla L, Zhang F, Wander C, Bao H, Yeh CY, Luo YJ, Olsen R, et al. (2020). Neuropeptides Modulate Local Astrocytes to Regulate Adult Hippocampal Neural Stem Cells. Neuron 108, 349–366.e6. 10.1016/j.neuron.2020.07.039. [PubMed: 32877641]
35. Yeh CY, Asrican B, Moss J, Quintanilla LJ, He T, Mao X, Cassè F, Gebara E, Bao H, Lu W, et al. (2018). Mossy Cells Control Adult Neural Stem Cell Quiescence and Maintenance through a Dynamic Balance between Direct and Indirect Pathways. Neuron 99, 493–510.e4. 10.1016/j.neuron.2018.07.010. [PubMed: 30057205]
36. Li YD, Luo YJ, Chen ZK, Quintanilla L, Cherasse Y, Zhang L, Lazarus M, Huang ZL, and Song J (2022). Hypothalamic modulation of adult hippocampal neurogenesis in mice confers activity-dependent regulation of memory and anxiety-like behavior. Nat. Neurosci. 25, 630–645. 10.1038/s41593-022-01065-x. [PubMed: 35524139]
37. Naumenko VS, Popova NK, Lacivita E, Leopoldo M, and Ponimaskin EG (2014). Interplay between serotonin 5-HT1A and 5-HT7 receptors in depressive disorders. CNS Neurosci. Ther. 20, 582–590. 10.1111/cns.12247. [PubMed: 24935787]
38. Bickmeyer U, Heine M, Manzke T, and Richter DW (2002). Differential modulation of I(h) by 5-HT receptors in mouse CA1 hippocampal neurons. Eur. J. Neurosci. 16, 209–218. 10.1046/j.1460-9568.2002.02072.x. [PubMed: 12169103]
39. Browne CA, Clarke G, Dinan TG, and Cryan JF (2011). Differential stress-induced alterations in tryptophan hydroxylase activity and serotonin turnover in two inbred mouse strains. Neuropharmacology 60, 683–691. 10.1016/j.neuropharm.2010.11.020. [PubMed: 21130784]
40. Torres ILS, Gamaro GD, Vasconcellos AP, Silveira R, and Dalmaz C (2002). Effects of chronic restraint stress on feeding behavior and on monoamine levels in different brain structures in rats. Neurochem. Res. 27, 519–525. 10.1023/a:1019856821430. [PubMed: 12199158]
41. Yun J, Koike H, Ibi D, Toth E, Mizoguchi H, Nitta A, Yoneyama M, Ogita K, Yoneda Y, Nabeshima T, et al. (2010). Chronic restraint stress impairs neurogenesis and hippocampus-dependent fear memory in mice: possible involvement of a brain-specific transcription factor Npas4. J. Neurochem. 114, 1840–1851. 10.1111/j.1471-4159.2010.06893.x. [PubMed: 20626564]

42. Barha CK, Brummelte S, Lieblich SE, and Galea LAM (2011). Chronic restraint stress in adolescence differentially influences hypothalamic-pituitary-adrenal axis function and adult hippocampal neurogenesis in male and female rats. Hippocampus 21, 1216–1227. 10.1002/hipo.20829. [PubMed: 20665592]
43. Ciranna L, and Catania MV (2014). 5-HT7 receptors as modulators of neuronal excitability, synaptic transmission and plasticity: physiological role and possible implications in autism spectrum disorders. Front. Cell. Neurosci. 8, 250. 10.3389/fncel.2014.00250. [PubMed: 25221471]
44. Altieri SC, Garcia-Garcia AL, Leonardo ED, and Andrews AM (2013). Rethinking 5-HT1A receptors: emerging modes of inhibitory feedback of relevance to emotion-related behavior. ACS Chem. Neurosci. 4, 72–83. 10.1021/cn3002174. [PubMed: 23336046]
45. Bonaguidi MA, Wheeler MA, Shapiro JS, Stadel RP, Sun GJ, Ming GL, and Song H (2011). In vivo clonal analysis reveals self-renewing and multipotent adult neural stem cell characteristics. Cell 145, 1142–1155. 10.1016/j.cell.2011.05.024. [PubMed: 21664664]
46. Snyder JS, Soumier A, Brewer M, Pickel J, and Cameron HA (2011). Adult hippocampal neurogenesis buffers stress responses and depressive behaviour. Nature 476, 458–461. 10.1038/nature10287. [PubMed: 21814201]
47. Goel N, Philippe TJ, Chang J, Koblanski ME, and Viau V (2022). Cellular and serotonergic correlates of habituated neuroendocrine responses in male and female rats. Psychoneuroendocrinology 136, 105599. 10.1016/j.psyneuen.2021.105599. [PubMed: 34891046]
48. Marcinkiewcz CA, Bierlein-De La Rosa G, Dorrier CE, McKnight M, DiBerto JF, Pati D, Gianessi CA, Hon OJ, Tipton G, McElligott ZA, et al. (2019). Sex-Dependent Modulation of Anxiety and Fear by 5-HT(1A) Receptors in the Bed Nucleus of the Stria Terminalis. ACS Chem. Neurosci. 10, 3154–3166. 10.1021/acschemneuro.8b00594. [PubMed: 31140276]
49. Encinas JM, and Enikolopov G (2008). Identifying and quantitating neural stem and progenitor cells in the adult brain. Methods Cell Biol. 85, 243–272. 10.1016/S0091-679X(08)85011-X. [PubMed: 18155466]
50. Schneider CA, Rasband WS, and Eliceiri KW (2012). NIH Image to ImageJ: 25 years of image analysis. Nat. Methods 9, 671–675. 10.1038/nmeth.2089. [PubMed: 22930834]
51. Song J, Zhong C, Bonaguidi MA, Sun GJ, Hsu D, Gu Y, Meletis K, Huang ZJ, Ge S, Enikolopov G, et al. (2012). Neuronal circuitry mechanism regulating adult quiescent neural stem-cell fate decision. Nature 489, 150–154. 10.1038/nature11306. [PubMed: 22842902]
52. Li YD, Luo YJ, Xie L, Tart DS, Sheehy RN, Zhang L, Coleman LG Jr., Chen X, and Song J (2023). Activation of hypothalamicenhanced adult-born neurons restores cognitive and affective function in Alzheimer's disease. Cell Stem Cell 30, 415–432.e6. 10.1016/j.stem.2023.02.006. [PubMed: 37028406]
53. Bao H, Asrican B, Li W, Gu B, Wen Z, Lim SA, Haniff I, Ramakrishnan C, Deisseroth K, Philpot B, and Song J (2017). Long-Range GABAergic Inputs Regulate Neural Stem Cell Quiescence and Control Adult Hippocampal Neurogenesis. Cell Stem Cell 21, 604–617.e5. 10.1016/j.stem.2017.10.003. [PubMed: 29100013]
54. Song J, Sun J, Moss J, Wen Z, Sun GJ, Hsu D, Zhong C, Davoudi H, Christian KM, Toni N, et al. (2013). Parvalbumin interneurons mediate neuronal circuitry-neurogenesis coupling in the adult hippocampus. Nat. Neurosci. 16, 1728–1730. 10.1038/nn.3572. [PubMed: 24212671]

Highlights

- Adult mouse Ascl1-NSCs express 5HT1ARs in females, while they express 5HT7Rs in males
- 5HT1AR deletion in Ascl1-NSCs of females impairs NSCs via upregulation of 5HT7Rs
- Stress upregulates 5HT7Rs in Ascl1-NSCs of females and reduces NSCs via 5HT1ARs
- Stress downregulates 5HT7Rs in Ascl1-NSCs of males, and NSCs are maintained

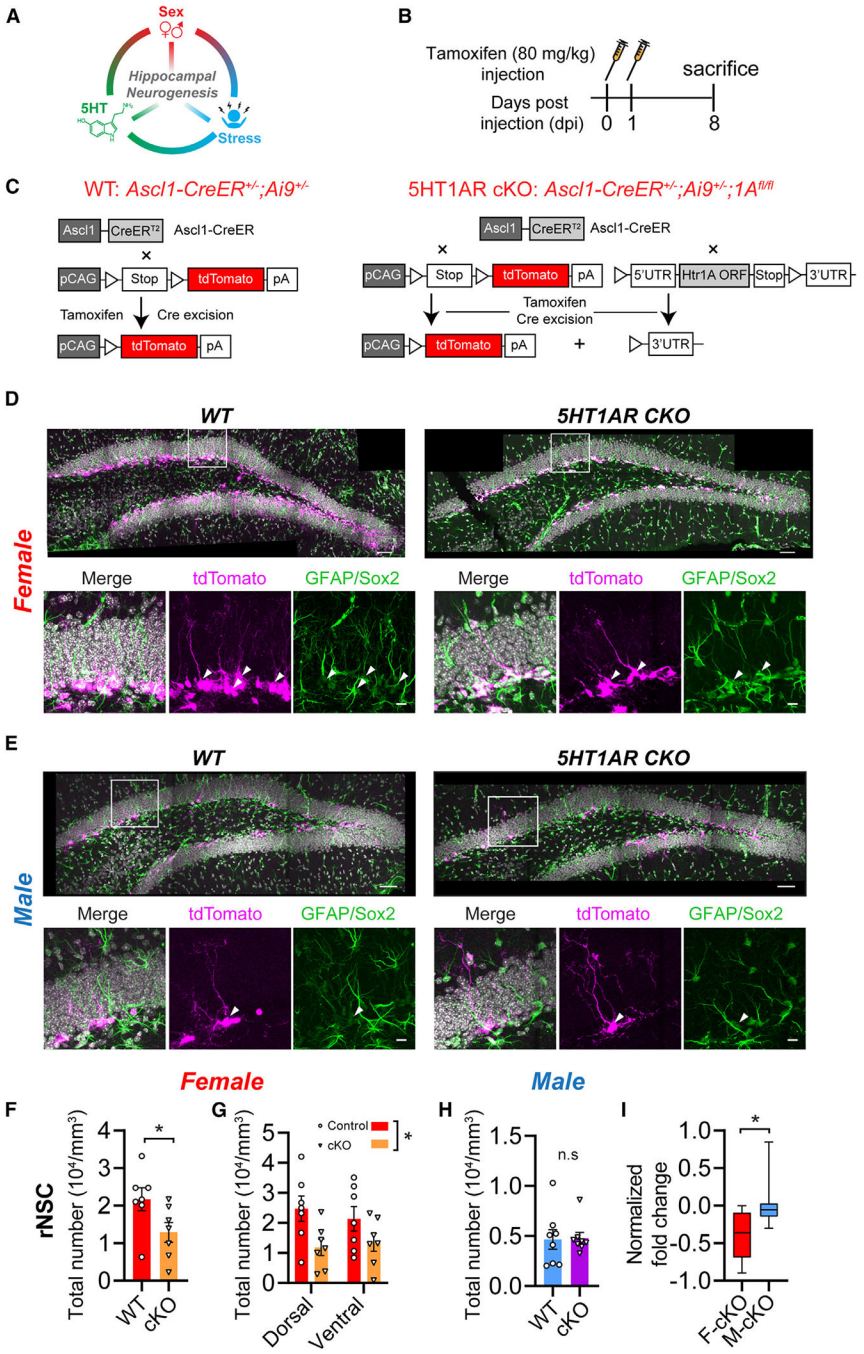

Figure 1. Selective deletion of 5HT1ARs in adult rNSCs decreases the rNSC pool in females

(A) Illustration of the hypothesis.

(B) Schematic of the experimental paradigm.

(C) Schematic of the Ascl1-CreER/Ai9 (WT, left), and Ascl1-CreER/htr1a$^{fl/fl}$/Ai9 (5HT1AR cKO, right) breeding strategy. White triangles indicate *loxP* sites. pA, polyadenylation signal. ORF, open reading frame.

(D) Sample images showing Ascl1-rNSCs with tdTomato, GFAP, and Sox2 markers in females. Scale bars, 50 μm. Enlarged images of the white box are shown below. Scale bars,

10 μm. The images were acquired using the stitching function of FV3000 and only the areas containing DG were imaged.

(E) Sample images showing Ascl1-rNSCs with tdTomato, GFAP, and Sox2 markers in males. Scale bars, 50 μm. Enlarged images of the white box are shown below. Scale bars, 10 μm.

(D and E) Arrowheads indicate Ascl1-rNSCs.

(F) Quantification of total numbers of Ascl1-rNSCs in WT or 5HT1AR cKO females (WT, cKO: 7, 7 mice; two-tailed unpaired t test, $t_{12} = 2.180$, $*p = 0.0499$).

(G) Quantification of dorsal/ventral Ascl1-rNSC numbers in WT or 5HT1AR cKO females (WT, cKO: 7, 7 mice; two-way repeated measures [RM] ANOVA, interaction: $F_{(1,12)} = 1.660$, $p = 0.2219$; dorsal/ventral: $F_{(1,12)} = 0.6596$, $p = 0.6596$; genotype: $F_{(1,12)} = 4.958$, $*p = 0.0459$).

(H) Quantification of total numbers of Ascl1-rNSCs in WT or 5HT1AR cKO males (WT, cKO: 8, 8 mice; two-tailed unpaired t test, $t_{14} = 0.1076$, $p = 0.9159$).

(I) Normalized fold change between females and males (female, male: 7, 8 mice; Mann-Whitney test, $*p = 0.0401$). Data are shown as mean ± SEM; $*p < 0.05$).

See also Figures S1 and S2.

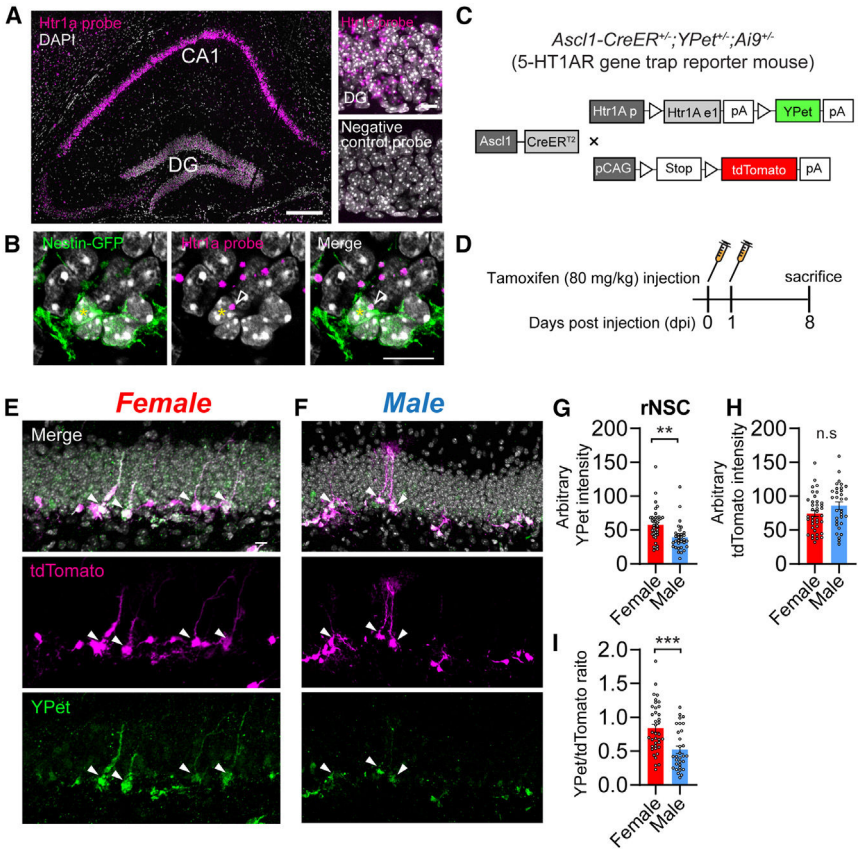

Figure 2. Adult rNSCs in females express 5HT1ARs

(A) Composite confocal image showing abundant 5HT1AR expression in the hippocampus. Scale bar, 200 μm. Magnified sample images for positive and negative probes are shown on the right. Scale bars, 10 μm.

(B) Sample images (single plane) showing 5HT1AR expressed in Nestin-GFP+ neural precursors. Yellow asterisks indicate Nestin-GFP+ somata. Arrowheads indicate the colocalization of Htr1a mRNA (magenta) with the nestin-GFP+ somata. Scale bar, 10 μm.

(C) Schematic of the Ascl1-YPet-Ai9 breeding strategy. White triangles indicate *loxP* sites. Htr1A p., 5ht1ar promoter; Htr1A e1, 5ht1ar exon.

(D) Schematic of the experimental paradigm.

(E) Sample images showing YPet and tdTomato expression in females. Scale bar, 10 μm.

(F) Sample images showing YPet and tdTomato expression in males. Scale bar, 10 μm. Arrowheads indicate Ascl1-rNSCs.

(G) Comparison of raw YPet expression in Ascl1-rNSCs (t_{67} = 3.372, $^{**}p$ = 0.0012).

(H) Comparison of raw tdTomato expression in Ascl1-rNSCs (t_{67} = 1.589, p = 0.1169).

(I) Normalized YPet expression (YPet/tdTomato) in Ascl1-rNSCs (t_{67} = 3.847, $^{***}p$ = 0.0003).

For (G)–(I), female, male: cells, n = 38, 31; animals, n = 4, 4. Two-tailed unpaired t test. Data are shown as mean ± SEM. $^{**}p < 0.01$, $^{***}p < 0.001$.

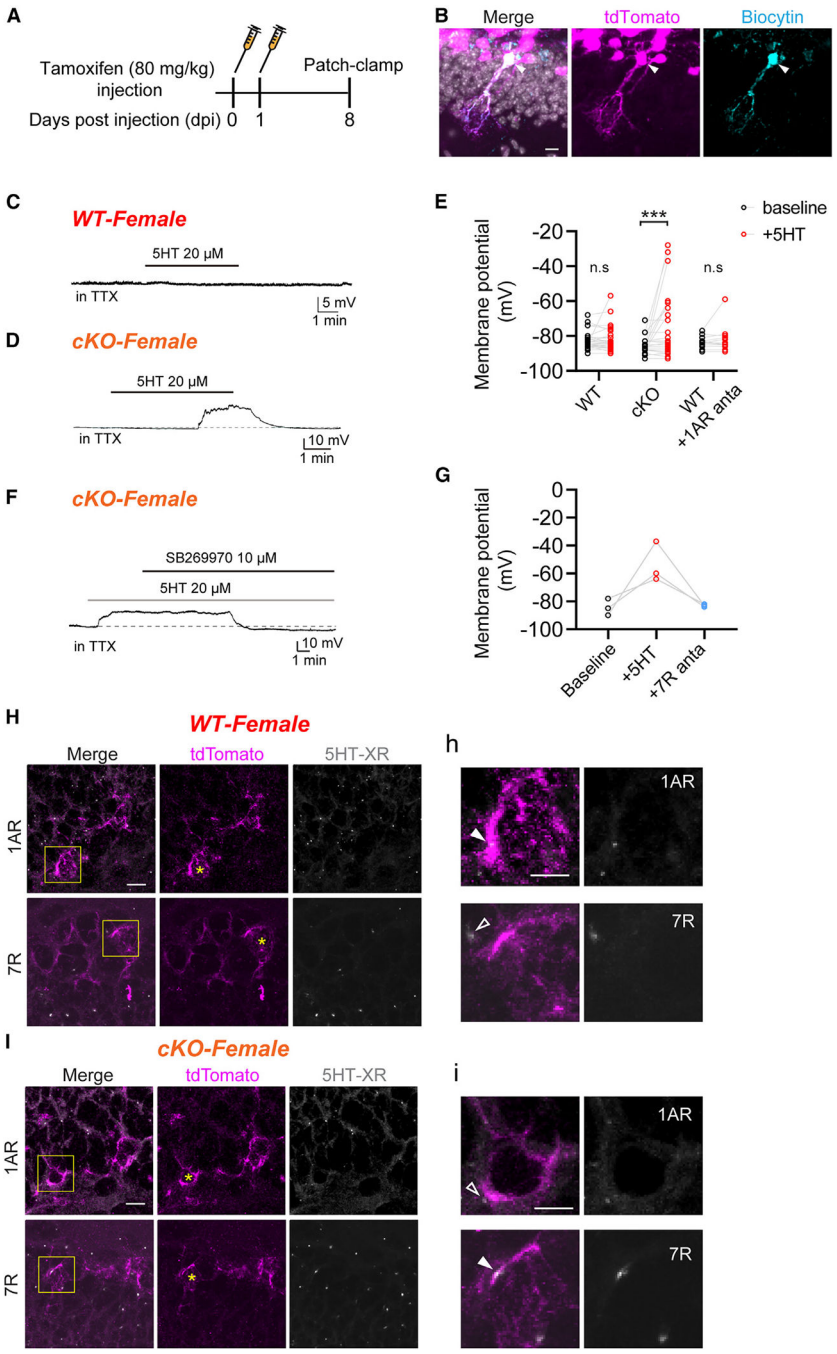

Figure 3. Deleting 5HT1ARs in rNSCs of females leads to upregulation of 5HT7Rs

(A) Schematic of the experimental paradigm for the patch-clamp study.

(B) Sample images of patched Ascl1-rNSCs from a hippocampal slice. Arrowheads indicate that the biocytin+ cell was also positive for tdTomato. Scale bar,10 μm.

(C and D) Sample traces showing changes in rNSC Vm to 5HT (20 μM) in the presence of 1 μM TTX in a WT female mouse (C) and a 5HT1AR cKO female mouse (D).

(E) Membrane potential (Vm) changes of rNSCs upon 5HT bath application in female WT mice, 5HT1AR cKO mice, and WT mice in the presence of the 5HT1AR antagonist (labeled

as 1AR anta). Each point represents a Vm value. WT, cKO, WT+1AR anta: n = 37, 24, 14 cells; 13, 8, 5 mice. Two-way RM ANOVA (interaction $F_{(2,72)}$ = 5.583, **p = 0.0056; group $F_{(2,72)}$ = 1.332, **p = 0.2704; time $F_{(2,72)}$ = 8.178, **p = 0.0055), followed by Sidak's multiple-comparisons test (F-WT: t_{72} = 0.2962, p = 0.9875; F-cKO: t_{72} = 4.384, ***p = 0.0001; F-WT+1AR anta: t_{72} = 0.4744, p = 0.9520). Data are shown as mean ± SEM.

(F) A representative trace showing that 5HT induced depolarization was completely washed out by the 5HT7R antagonist (SB-269970 10 μM) in a 5HT1AR cKO female mouse.

(G) Changes of rNSC Vm at baseline, during 5HT, and then with 5HT + 5HT7R antagonist (n = 3 cells, 2 mice).

(H) Sample confocal images showing 5HT1AR and 7R expression in Ascl1-rNSCs of WT females. Scale bar, 10 μm.

(h) Magnified images of the yellow box corresponding to (H). Scale bar, 5 μm. A white solid arrowhead indicates that 5HT1AR mRNA is colocalized with the Ascl1-rNSC, a white hollow arrowhead indicates that 5HT7R mRNA does not overlap with the Ascl1-rNSC, and yellow asterisks indicate Ascl1-rNSC somata.

(I) Sample confocal images showing 5HT1AR and 7R expression in Ascl1-rNSCs of 5HT1AR cKO females. Scale bar, 10 μm.

(i) Magnified images of the yellow box corresponding to (I). Scale bar, 5 μm. A white solid arrowhead indicates that 5HT7R mRNA is colocalized with the Ascl1-rNSC, a white hollow arrowhead indicates that 5HT1AR mRNA does not overlap with the Ascl1-rNSC, and yellow asterisks indicate Ascl1-rNSC somata.

See also Figure S3.

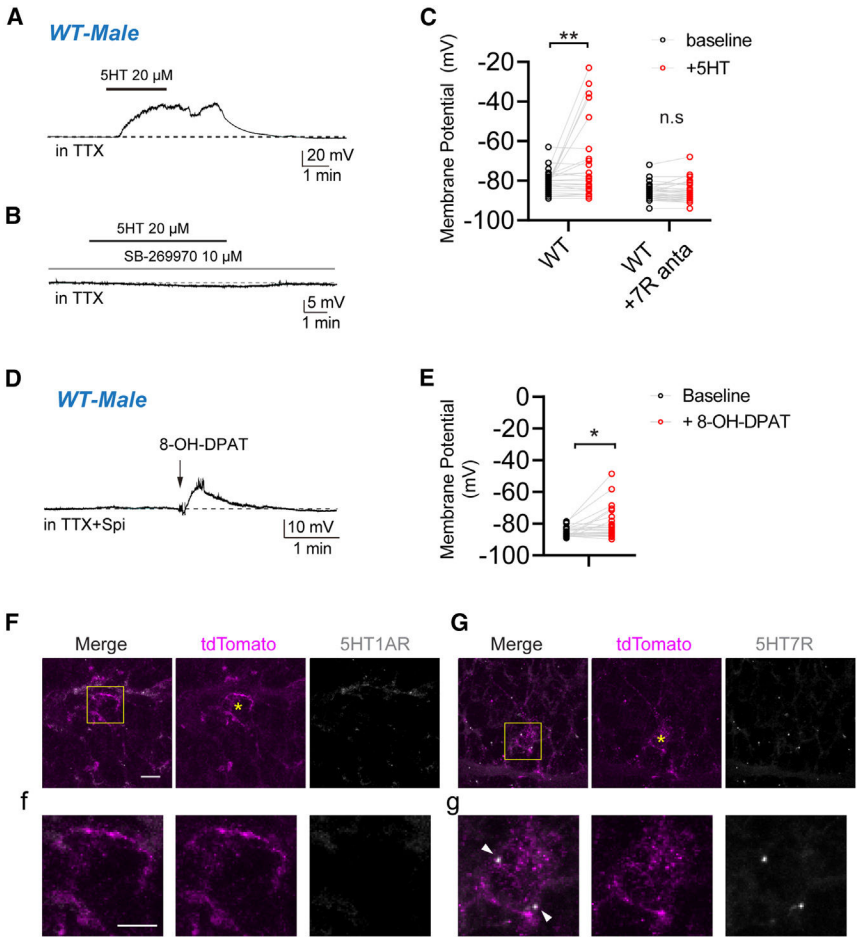

Figure 4. Adult rNSCs in males express 5HT7Rs

(A) A sample trace showing that 5HT (20 μM) bath application induced a robust depolarization in the presence of 1 μM TTX in a WT male mouse.

(B) A sample trace showing that pre-treatment withthe 5HT7R antagonist (SB-269970, 10 μM) completely blocked 5HT-induced depolarization in the presence of 1 μM TTX in a WT male mouse.

(C) Vm changes of rNSCs upon 5HT bath application in the absence or presence of the 5HT7R antagonist (labeled as 7R anta) in WT males. Each point represents a Vm value. WT, WT+7R anta: $n = 34$, 36 cells; 15, 10 mice. Two-way RM ANOVA (interaction $F_{(1,68)} = 6.629$, $^{*}p = 0.0122$; group $F_{(1,68)} = 15.40$, $^{***}p = 0.0002$; time $F_{(1,68)} = 6.318$, $^{*}p = 0.0143$), followed by Sidak's multiple-comparisons test (M-WT: $t_{68} = 3.548$, $^{**}p = 0.0014$; M-WT+1AR anta: $t_{68} = 0.0434$, $p = 0.9988$).

(D) A representative trace showing that spike application of 8-OH-DPAT, a mixed 5HT1A/5HT7 receptor agonist, depolarized an rNSC in the presence of both TTX (1 μM) and the 5HT1AR antagonist (spi [spiroxatrine], 1 μM) in a WT male mouse.

(E) Vm changes of rNSCs to spike application of8-OH-DPAT in the presence of TTX 1 μM+5HT1AR antagonist in WT males ($n = 25$ cells, 5 mice; paired Student's t test, $^{*}p = 0.0107$).

(F) Sample confocal images showing 5HT1AR expression in Ascl1-rNSCs of WT males. Scale bar, 10 μm. (f) Magnified images of the yellow box corresponding to (F). Scale bar, 5 μm (a yellow asterisk indicates the Ascl1-rNSCs soma).
(G) Sample confocal images showing 5HT7R expression in Ascl1-rNSCs of WT males. Scale bar, 10 μm. (g) Magnified images of the yellow box corresponding to (G). Scale bar, 5 μm. White solid arrowheads indicate that 5HT7R mRNA are colocalized in the Ascl1-rNSCs somata, and a yellow asterisk indicates the Ascl1-rNSCs soma).
Data are shown as mean ± SEM. *$p < 0.05$, **$p < 0.01$, ***$p < 0.001$.

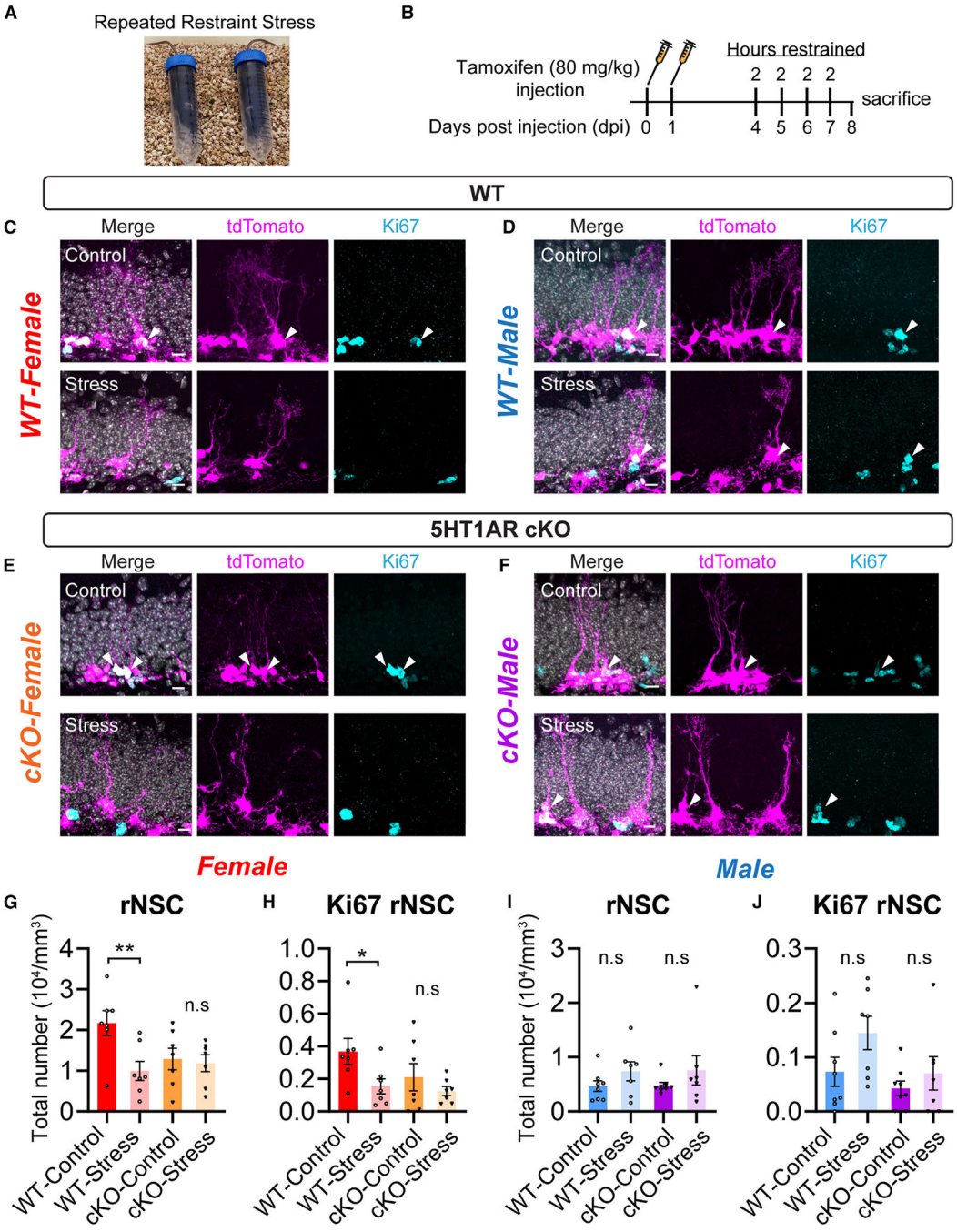

Figure 5. 5HT1ARs mediate stress vulnerability of rNSCs in females

(A) Experimental apparatus for the RRS mouse model.

(B) Schematic of the experimental paradigm.

(C–F) Sample images showing Ascl1-rNSC in WT/cKO from both sexes under control or stress conditions. Scale bar, 20 μm. Arrowheads indicate Ascl1-rNSCs.

(G) Quantification of total number of Ascl1-rNSCs in female WT or 5HT1AR cKO mice under control and stress conditions. $n = 7$ mice per group. Two-way ANOVA (interaction $F_{(1,24)} = 4.397$, $^*p = 0.0467$; treatment $F_{(1,24)} = 6.210$, $^*p = 0.0200$; genotype $F_{(1,24)} =$

1.828, $p = 0.1890$), followed by Sidak's multiple-comparisons test ([WT-control vs. WT-stress) $t_{24} = 3.245$, $^{**}p = 0.0069$; [cKO-control vs. cKO-stress] $t_{24} = 0.2794$, $p = 0.9526$). (H) Quantification of total number of Ki67+ Ascl1-rNSCs in female WT or 5HT1AR cKO mice under control and stress conditions. $n = 7$ mice per group. Two-way ANOVA (interaction $F_{(1,24)} = 1.043$, $p = 0.3174$; treatment $F_{(1,24)} = 5.589$, $^{*}p = 0.0265$; genotype $F_{(1,24)} = 2.394$, $p = 0.1502$), followed by Sidak's multiple-comparisons test ([WT-control vs. WT-stress] $t_{24} = 2.264$, $^{*}p = 0.0248$; [cKO-control vs. cKO-stress] $t_{24} = 0.9497$, $p = 0.3517$). (I) Quantification of total number of Ascl1-rNSCs in male WT or 5HT1AR cKO mice under control and stress conditions. n = 7–8 mice per group. Two-way ANOVA (interaction $F_{(1,26)} = 0.0004828$, $p = 0.9826$; treatment $F_{(1,26)} = 2.981$, $p = 0.0961$; genotype $F_{(1,26)} = 0.009578$, $p = 0.9228$), followed by Sidak's multiple-comparisons test ([WT-control vs. WT-stress] $t_{26} = 1.205$, $p = 0.4208$; [cKO-control vs. cKO-stress] $t_{26} = 1.236$, $p = 0.4031$). (J) Quantification of total number of Ki67+ Ascl1-rNSCs in male WT or 5HT1AR cKO mice under control and stress conditions. n = 7–8 mice per group. Two-way ANOVA (interaction $F_{(1,26)} = 0.7223$, $p = 0.4031$; treatment $F_{(1,26)} = 3.663$ $p = 0.0667$; genotype $F_{(1,26)} = 4.103$, $p = 0.0532$), followed by Sidak's multiple comparisons test ([WT-control vs. WT-stress] $t_{26} = 1.954$, $p = 0.1192$; [cKO-control vs. cKO-stress] $t_{26} = 0.7524$, $p = 0.7068$). Data are shown as mean ± SEM. $^{*}p < 0.05$, $^{**}p < 0.01$. See also Figure S5.

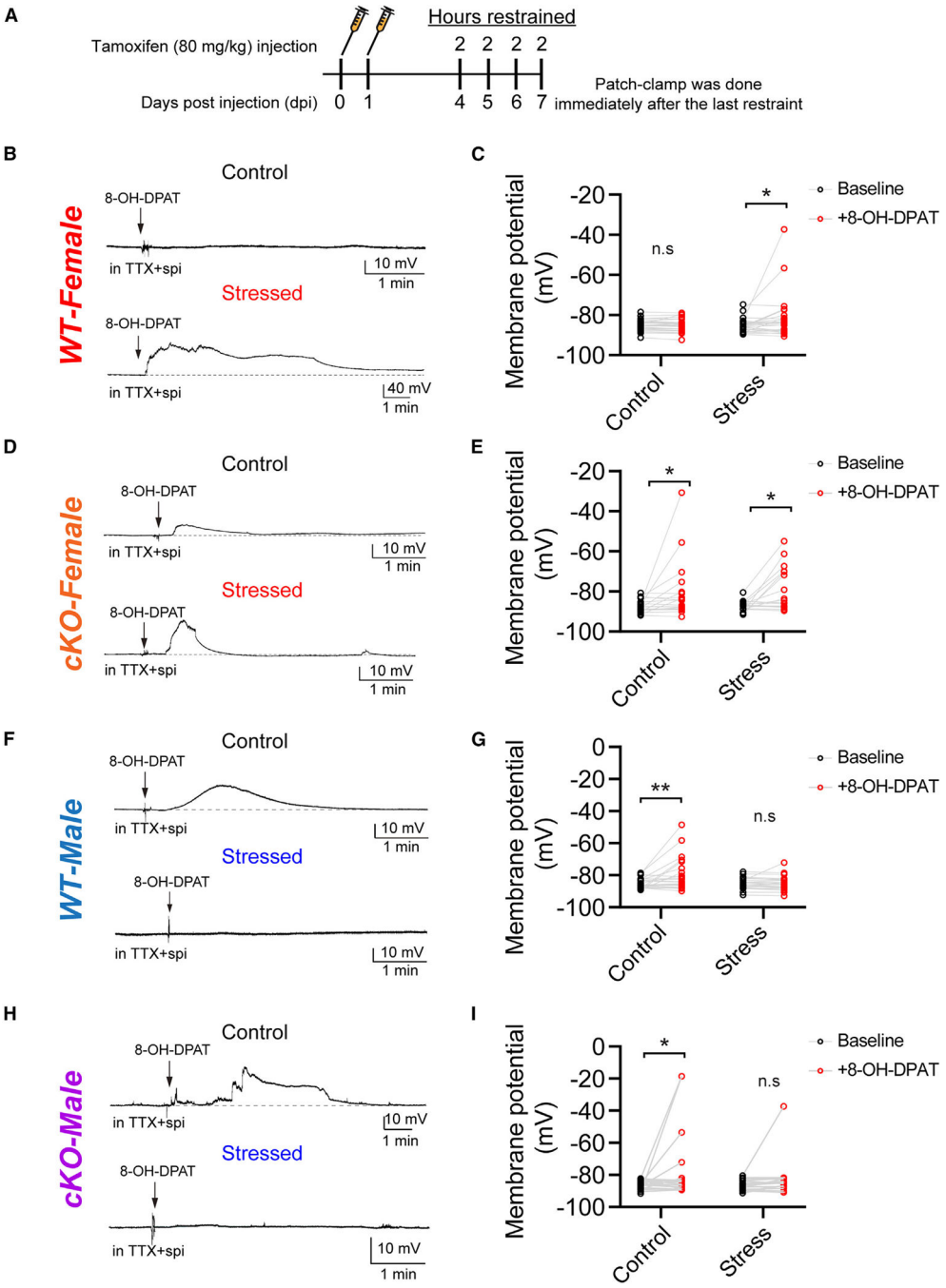

Figure 6. Stress upregulates 5HT7Rs in adult rNSCs of females through 5HT1ARs but downregulates 5HT7Rs in adult rNSCs of males independent of 5HT1Ars

(A) Schematic of the experimental paradigm.

(B) Sample traces showing that spike application of 8-OH-DPAT in the presence of both TTX (1 μM) and the 5HT1AR antagonist (spi, 1 μM) did not affect Vm of an Ascl1-rNSC in a control WT female (top) but induced a big and long-lasting depolarization of a Ascl1-rNSC in a stressed WT female (bottom).

(C) Vm changes of Ascl1-rNSCs upon spike application of 8-OH-DPAT in the presence of TTX (1 μM)+5HT1AR antagonist in control and stressed female WT mice (WT-control,

WT-stress: $n = 28$, 26 cells; 6, 6 mice. Two-way RM ANOVA, interaction $F_{(1,52)} = 3.636$, $p = 0.0621$; group $F_{(1,52)} = 0.2683$, $p = 0.0621$; treatment $F_{(1,52)} = 0.2683$, $p = 0.0621$), followed by Sidak's multiple-comparisons test (WT-control $t_{52} = 0.0192$, $p = 0.9988$; WT-stress $t_{52} = 2.630$, $^{*}p = 0.0223$).

(D) Sample traces showing that spike application of 8-OH-DPAT in the presence of both TTX (1 μM) and 5HT1AR antagonist (spi, 1 μM) induced a Vm depolarization of Ascl1-rNSCs in a control cKO female (top) and a stressed cKO female (bottom).

(E) Vm changes of Ascl1-rNSCs upon spike application of 8-OH-DPAT in the presence of TTX (1 μM)+5HT1AR antagonist in control and stressed 5HT1AR cKO females. WT-control, WT-stress: $n = 19$, 18 cells; 5, 4 mice (two-way RM ANOVA, interaction $F_{(1,35)} = 0.0453$, $p = 0.8328$; group $F_{(1,35)} = 0.0565$, $p = 0.8135$; treatment $F_{(1,35)} = 12.20$, $^{**}p = 0.0013$), followed by Sidak's multiple-comparisons test (cKO-control $t_{35} = 2.351$, $^{*}p = 0.0484$; cKO-stress $t_{35} = 2.585$, $^{*}p = 0.0279$).

(F) Sample traces showing that spike application of 8-OH-DPAT in the presence of both TTX (1 μM) and 5HT1AR antagonist (spi, 1 μM) induced a Vm depolarization of a Ascl1-rNSCs in a control WT male (top) but did not affect Vm of a Ascl1-rNSCs in a stressed WT male (bottom).

(G) Vm changes of Ascl1-rNSCs upon spike application of 8-OH-DPAT in the presence of TTX (1 μM)+5HT1AR antagonist in control and stressed male WT mice (WT-control, WT-stress: $n = 25$, 22 cells; 5, 4 mice. Two-way RM ANOVA, interaction $F_{(1,45)} = 5.763$, $^{*}p = 0.0206$; group $F_{(1, 45)} = 2.504$, $p = 0.1206$; treatment $F_{(1, 45)} = 6.732$, $^{*}p = 0.0127$), followed by Sidak's multiple-comparisons test (WT-control $t_{45} = 3.651$, $^{**}p = 0.0014$; WT-stress $t_{45} = 0.1330$, $p = 0.9889$). The WT-control dataset was the same as shown in Figure 4E (included here for cross-comparison with the WT-stress dataset).

(H) Sample traces showing that spike application of 8-OH-DPAT in the presence of both TTX (1 μM) and 5HT1AR antagonist (spi, 1 μM) induced a Vm depolarization of Ascl1-rNSCs in a control cKO male (top) and a stressed cKO male (bottom).

(I) Vm changes of Ascl1-rNSCs upon spike application of 8-OH-DPAT in the presence of TTX (1 μM)+5HT1AR antagonist in control and stressed 5HT1AR cKO males (cKO-control, cKO-stress: $n = 20$, 17 cells; 6, 6 mice. Two-way RM ANOVA, interaction $F_{(1,35)} = 0.9081$, $p = 0.3471$; group $F_{(1,35)} = 0.7005$ $p = 0.4083$; treatment $F_{(1,35)} = 4.955$, $^{*}p = 0.0325$), followed by Sidak's multiple-comparisons test (cKO-control $t_{35} = 2.345$, $^{*}p = 0.0490$; cKO-stress $t_{35} = 0.8658$, $p = 0.6309$).

Data are shown as mean ± SEM. $^{*}p < 0.05$, $^{**}p < 0.01$.

KEY RESOURCES TABLE

REAGENT or RESOURCE	SOURCE	IDENTIFIER
Antibodies		
Goat anti-GFP	Rockland	Cat# 600–101-215; RRID: AB_218182
Rabbit anti-Ki67	Thermo fisher scientific	Cat# PA519462; RRID:AB_10981523
Mouse anti-GFAP	Millipore	Cat# IF03L; RRID: AB_212974
Goat anti-Sox2	Santa Cruz Biotechnology	Cat# sc-54517; RRID: AB_2195807
Rabbit dsRed primary antibody	Takara	Cat# 632496; RRID: AB_10013483
Alexa 488 anti-Rabbit secondary antibody	Thermo fisher Scientific	RRID: AB_2535792
Alexa 647 anti-Goat secondary antibody	Thermo fisher Scientific	RRID: AB_2535864
Alexa 647 anti-Mouse secondary antibody	Thermo fisher Scientific	RRID: AB_162542
Streptavidin conjugated to Alexa 647	Invitrogen	Cat# S32357
Fab fragment Unconjugated Donkey Anti-Mouse IgG (H + L) blocking antibody	Jackson Immunoresearch	Cat# 715–007-003; RRID: AB_2307338
4’,6-Diamidino-2-Phenylindole (DAPI)	Thermo fisher scientific	Cat# D1306; RRID: AB_2629482
Anti-fade reagent Fluorogel II with DAPI	Electron Microscopy Sciences	Cat# 17985–50
Chemicals, peptides, and recombinant proteins		
Biocytin	Sigma Aldrich	Cat# B4261
Serotonin hydrochloride	Tocris	Cat# 3547
Spiroxatrine	Tocris	Cat# 0631
SB 269970	Tocris	Cat# 1612
8-Hydroxy-DPAT hydrobromide	Tocris	Cat# 0529
Tetrodotoxin	Tocris	Cat# 1069
Tamoxifen	Sigma Aldrich	Cat# T5648
Critical commercial assays		
RNAscope 2.5 HD Reagent Kit-RED	Advanced Cell Diagnostics	Cat# 322350
RNAscope Fluorescent Multiplex V2 Kit	Advanced Cell Diagnostics	Cat# 323110
Experimental models: Organisms/strains		
C57BL/6J mice	Jackson laboratory	Stock No: 000664
Floxed 5HT1A-YPet mice	Generously shared by Dr. Rene Hen, Columbia University	(Samuels et al.)[20]
Floxed 5HT1AR mice	Generated by the Delpire lab at Vanderbilt, shared by Dr. Thomas Kash at UNC-CH	(Marcinkiewcz et al.)[48]
Nestin-GFP mice	(Encinas et al.)[49]	https://www.informatics.jax.org/allele/MGI:5523870
Ascl1CreER (B6, Ascl1$^{tm1.1(cre/ERT2)Jejo}$) mice	Jackson laboratory	Stock No: 012882
Ai9 (B6, Gt(ROSA)26Sor$^{tm9(CAG-tdTomato)Hze}$) mice	Jackson laboratory	Stock No: 007909
Oligonucleotides		

REAGENT or RESOURCE	SOURCE	IDENTIFIER
Mm-Htr1a Probe	Advanced Cell Diagnostics	Cat# 312301
Mm-Htr7 Probe	Advanced Cell Diagnostics	Cat# 401321
Negative Control Probe	Advanced Cell Diagnostics	Cat# 310043
Software and algorithms		
ImageJ	(Schneider et al.)[50]	https://ImageJ.net; RRID:SCR_003070
FV3000	Olympus	RRID:SCR_017015
Prism	GraphPad	RRID:SCR_002798
Imaris	Bitplane	RRID: SCR_007370
pClamp	Molecular Devices	RRID: SCR_011323